NAVAL POSTGRADUATE SCHOOL
Monterey, California

THESIS

CALIBRATION AND INITIALIZATION OF THE NPS MODIFIED INFRARED SEARCH AND TARGET DESIGNATION (IRSTD) SYSTEM

by

Gary Robert Ayers

December 1987

Thesis Advisor: Alfred W. Cooper

SECURITY CLASSIFICATION OF THIS PAGE

REPORT DOCUMENTATION PAGE

1a REPORT SECURITY CLASSIFICATION UNCLASSIFIED	1b RESTRICTIVE MARKINGS
2a SECURITY CLASSIFICATION AUTHORITY	3 DISTRIBUTION/AVAILABILITY OF REPORT Approved for public release; distribution is unlimited.
2b DECLASSIFICATION/DOWNGRADING SCHEDULE	
4 PERFORMING ORGANIZATION REPORT NUMBER(S)	5 MONITORING ORGANIZATION REPORT NUMBER(S)
6a NAME OF PERFORMING ORGANIZATION Naval Postgraduate School 6b OFFICE SYMBOL (If applicable) 61	7a NAME OF MONITORING ORGANIZATION Naval Postgraduate School
6c ADDRESS (City, State, and ZIP Code) Monterey, California 93943-5100	7b ADDRESS (City, State, and ZIP Code) Monterey, California 93943-5100
8a NAME OF FUNDING/SPONSORING ORGANIZATION 8b OFFICE SYMBOL (If applicable)	9 PROCUREMENT INSTRUMENT IDENTIFICATION NUMBER
8c ADDRESS (City, State, and ZIP Code)	10 SOURCE OF FUNDING NUMBERS PROGRAM ELEMENT NO / PROJECT NO / TASK NO / WORK UNIT ACCESSION NO

11 TITLE (Include Security Classification)
CALIBRATION AND INITIALIZATION OF THE NPS MODIFIED INFRARED SEARCH AND TARGET DESIGNATION (IRSTD) SYSTEM

12 PERSONAL AUTHOR(S)
Ayers, Gary Robert

13a TYPE OF REPORT	13b TIME COVERED	14 DATE OF REPORT (Year, Month, Day)	15 PAGE COUNT
Master's Thesis	FROM _____ TO _____	1987 December	93

16 SUPPLEMENTARY NOTATION

17 COSATI CODES		
FIELD	GROUP	SUB-GROUP

18 SUBJECT TERMS (Continue on reverse if necessary and identify by block number)
ADM, AN/SAR-8, Calibration, Collimator, Detector, Infrared, IR, IRSTD, Lead and Lag Arrays, Liquid Nitrogen

19 ABSTRACT (Continue on reverse if necessary and identify by block number)

The AN/SAR-8 IRSTD Advanced Development Model (ADM) at NPS was modified and put in partial operation. This work presents the results obtained in calibration of the relative responsivity of the individual detector sensor elements with their associated electronic system. The calibration was accomplished by projecting a parallel beam from a parabolic mirror 124.7 ± 1.0 cm from the telescopic input aperture using a collimated blackbody source system. This source was at a temperature of 500 ± 3.0 °C. This procedure revealed that the average amplitude response was 1.709 ± 0.102 volts for the lead array and 3.184 0.158 volts for the lag array. Seven detectors on the lead array and eight detectors on the lag array were found to be non-functional with another three detectors on the lag array performing at levels
(Continued)

20 DISTRIBUTION/AVAILABILITY OF ABSTRACT ☒ UNCLASSIFIED/UNLIMITED ☐ SAME AS RPT ☐ DTIC USERS	21 ABSTRACT SECURITY CLASSIFICATION UNCLASSIFIED
22a NAME OF RESPONSIBLE INDIVIDUAL Alfred W. Cooper	22b TELEPHONE (Include Area Code) (408) 646-2452 22c OFFICE SYMBOL 61Cr

DD FORM 1473, 84 MAR 83 APR edition may be used until exhausted
All other editions are obsolete

SECURITY CLASSIFICATION OF THIS PAGE

19. (Continued)

below standard. This modified system was found to be operating at a level of performance comparable to the original ADM configuration.

Approved for public release; distribution is unlimited.

Calibration and Initialization of the NPS Modified Infrared Search and Target Designation (IRSTD) System

by

Gary Robert Ayers
Lieutenant, United States Naval Reserve
B.S., Lambuth College, 1982

Submitted in partial fulfillment of the
requirements for the degree of

MASTER OF SCIENCE IN PHYSICS

from the

NAVAL POSTGRADUATE SCHOOL
December 1987

ABSTRACT

The AN/SAR-8 IRSTD Advanced Development Model (ADM) at NPS was modified and put in partial operation. This work presents the results obtained in calibration of the relative responsivity of the individual detector sensor elements with their associated electronic system. The calibration was accomplished by projecting a parallel beam from a parabolic mirror 124.7 ± 1.0 cm from the telescopic input aperture using a collimated blackbody source system. The source was at a temperature of 500 ± 3.0 °C. This procedure revealed that the average amplitude response was 1.709 ± 0.102 volts for the lead array and 3.184 ± 0.158 volts for the lag array. Seven detectors on the lead array and eight detectors on the lag array were found to be non-functional with another three detectors on the lag array performing at levels below standard. This modified system was found to be operating at a level of performance comparable to the original ADM configuration.

TABLE OF CONTENTS

ACKNOWLEDGEMENTS

The author would like to take this time to extend his deep felt appreciation to the people who have offered generously of their time and experience without which the completion of this thesis would have been improbable.

Mr. W. J. Lentz provided a vital source of technical knowledge and sweat of brow which proved invaluable in the setup of the ADM as well as innumerable related hardware and software items. Professor A. W. Cooper furnished, as thesis advisor, a supply of never ending faith which was vital in the continuance of studies and work.

A special thanks to Professor Eugene C. Crittenden for his patience, guidance, enlightenment, yachting skills, and always being there when needed.

Finally, my family (Jovette, Christopher, and Kyle) contributed the most by allowing me to do the work unencumbered with guilt and only nagging to finish this thesis at those times when it was critically needed.

This work was funded in part by Naval Sea Systems Command (SEA06W1-4) AN/SAR-8 Project Office under funding document N0002487WR10825 assigned to the Naval Academic Center for Infrared Technology (NACIT).

I. INTRODUCTION

In an age when the threats to naval surface combatants continue to become more sophisticated, current and evolving surveillance and designation systems must be improved to meet those threats. The use of infrared (IR) radiation for the detection of targets and weapon control has led to a series of developments analogous to radar during World War II. The U.S. Navy has long recognized the potential of an Infrared Search and Target Designation System (IRSTD) for providing passive detection and tracking of targets (i.e. surface vessels, aircraft, and anti-ship missiles) based on their self-radiated IR energy, especially under the strict requirements for systems that function under conditions of emissions control (EMCON). The AN/SAR-8, currently in the Engineering Development Phase, is an example of such an IRSTD. Since it is relatively immune to the adverse effects of many of the evolving threats, its development and installation is crucial to the survivability of naval surface combatants.

In January of 1984, the Advanced Development Model (ADM) of the AN/SAR-8 was sent to the Naval Academic Center for Infrared Technology (NACIT) located at the Naval Postgraduate School (NPS) in Monterey, California. Its primary use is to act not only as a learning tool for the

NPS students but also as a research and development tool in the advancing IRSTD program. After extensive refurbishment and modification, this system will be used to create a background data base in order to test new track and background suppression processing algorithms. Because of the modifications and repairs and in order to ensure an accurate data base, the NPS IRSTD had to be calibrated. This thesis constitutes the insitu calibration of the detector array of the NPS IRSTD after the performance of several necessary tasks which were essential to the start up of the IRSTD system.

This thesis is organized as follows:

* Section II is an introduction to and general discussion of the AN/SAR-8 IRSTD system.
* Section III gives a description of the equipment and procedure used in collecting calibration data.
* Section IV gives an analysis of the data obtained from the calibration of the detector array.
* Section V is a discussion of the conclusions with recommendations for the future.
* Appendix A is a review of IR theory including radiation theory, sources, atmospheric propagation, and detectors.
* Appendix B contains graphs of several detectors' responses to a collimated IR source.
* Appendix C is a comparison of the temperature versus time curves for the ADM and NPS IRSTD systems.
* Appendix D is a comparison of the IR background to a visual photograph of the same area.
* Appendix E is a photograph of the panoramic view as seen from the final installed site for the AN/SAR-8.

II. AN/SAR-8 IRSTD

A. GENERAL

The AN/SAR-8 is a passive IRSTD system designed to detect and track air and surface targets at tactically useful ranges by exploiting the IR signature generated by missile and aircraft plumes and aerodynamically heated surfaces. It acts as a ship's sensor in addition to installed radar, electronic support measures (ESM) and visual systems. The SAR-8 allows operation in environments which would be inherently adverse to existing sensor systems, such as radio frequency (RF) jamming, EMCON and heavy clutter conditions. It also can pick up those hard to detect targets which have a low radar cross-section (RCS), low flight profiles and high speed (i.e. anti-ship cruise missiles).

The system's primary functions are to provide continuous air and surface search capabilities, detection and designation of targets and track-while-scan of multiple air targets.

Secondary functions include passive navigational aid for station keeping, passive range and classification of surface targets and collision avoidance.

B. PROGRAM HISTORY

IR sensor systems are not a new concept to the scientific community. However, recent technological advances in the areas of computer hardware, solid-state integrated circuits, IR sensitive materials and new signal processing techniques, were needed to lay the foundations for the present IRSTD systems. The following is a chronological list of events which led to the present IRSTD:

* In 1960, the U.S. Navy sponsored development and testing of the Infrared Electronic Warfare System (IREWS).
* IRST (first test version on the IRSTD) prototype testing took place by Spar in 1969.
* In 1974, the Canadian Navy sponsored the development and testing of the Shipboard Passive Surveillance and Detection System (SPSDS).
* The U.S. Navy posted the operational requirement for a passive IRST system in 1975.
* A U.S.-Canadian Memorandum of Understanding and a Joint Project Agreement was signed in 1976 which resulted in the actual contracting and construction of the Advanced Development Model (ADM) of the IRST system.
* In May of 1978 the IRST system was tested in Halifax, Nova Scotia.
* In June of 1978 the IRST went aboard HMCS ALGONQUIN for at-sea shake down and further testing,
* In April of 1979 the ADM was moved to Key West, Florida for further testing and program validation.
* Upon completion of the Key West testing, OPTEVFOR recommended full scale engineering development of the IRST/IRSTD. The system was then transferred to the USS Kinkaid, in September of 1979, for continued testing and developmental considerations.
* After the trial the ADM was sent to the Naval Surface Weapons Center (NSWC) at Dahlgren, Virginia.

* Full scale Engineering Development was approved in June of 1981.

* In 1983 a subsequent Joint Agreement was signed by the U.S. and Canada for the engineering development of the IRSTD system.

* The prime contract was signed with SPAR and General Electric in August 1984.

* In January of 1985, the ADM was transferred to NACIT at NPS in Monterey, California to be used in research.

When the ADM arrived at NPS, it was found to be in a state of disrepair. Major modifications of the system were needed in order to make it operational, in particular the replacing of the double-wall vacuum dewar cooling system with a single-wall foam insulated one [Ref. 1]. Most of the modifications have been completed with the exception of installation of Analog-to-Digital converters and various cabling to transmit multiplexed data from the ADM to a remote Masscomp minicomputer. Also needed is the computer programming which will take the stored data and display it on a screen.

C. AN/SAR-8 ADM DESCRIPTION

The IRSTD system is made up of a collection of several interwoven subsystems. The subsystems can be divided into two general groups of (above-decks and below-decks) equipment. Figure 1 shows the ADM as it was configured on the USS Kinkaid. The above-decks equipment consisted of the

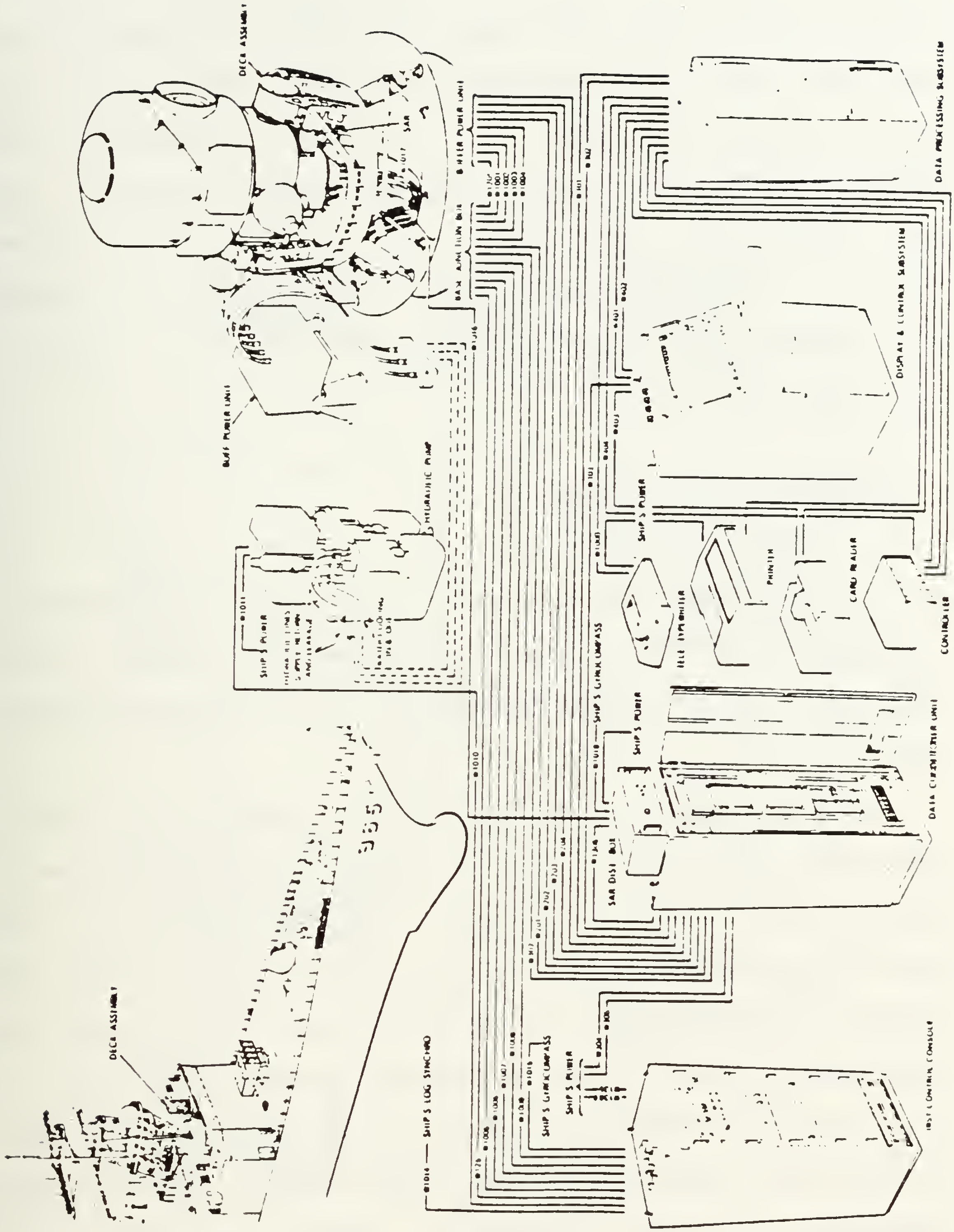

Figure 1. ISRTD Onboard USS Kinkaid

Scanner Assembly and slip rings, the Stable Platform, Buffer Power Unit (BPU), and associated junction boxes. The below-decks equipment consists of the Scanner Assembly Control Console (SACC), the Stable Platform Control Console, the Data Conditioner Unit (DCU), the Data Processing System (DPS), and the Display and Control System (DCS). An overall block diagram of the various subsystems appears in Figure 2. [Ref. 2]

D. SUBSYSTEM DESCRIPTIONS

1. Sensor Subsystem

This subsystem comprises a Schmidt reflecting telescope, infrared detectors, bandwidth filters, flat conducting cables, pre-amplifiers and a cooling system. [Ref. 3]

The optics consist of an F/1 Schmidt catadioptric telescope with a 10 inch entrance aperture using an aspheric corrector plate made of germanium. The reflector is a 16.625 inch aluminum mirror mounted by its back. This focuses the incident energy onto the detector head which hangs down stalk-like in front of the reflector as shown in Figure 3. This necessary structure results in an obscuration of part of the input aperture. The NPS IRSTD version has the added capability of being focused by moving the sensor probe toward or away from the reflector. This capability was achieved by the removal of alignment pins and a germanium

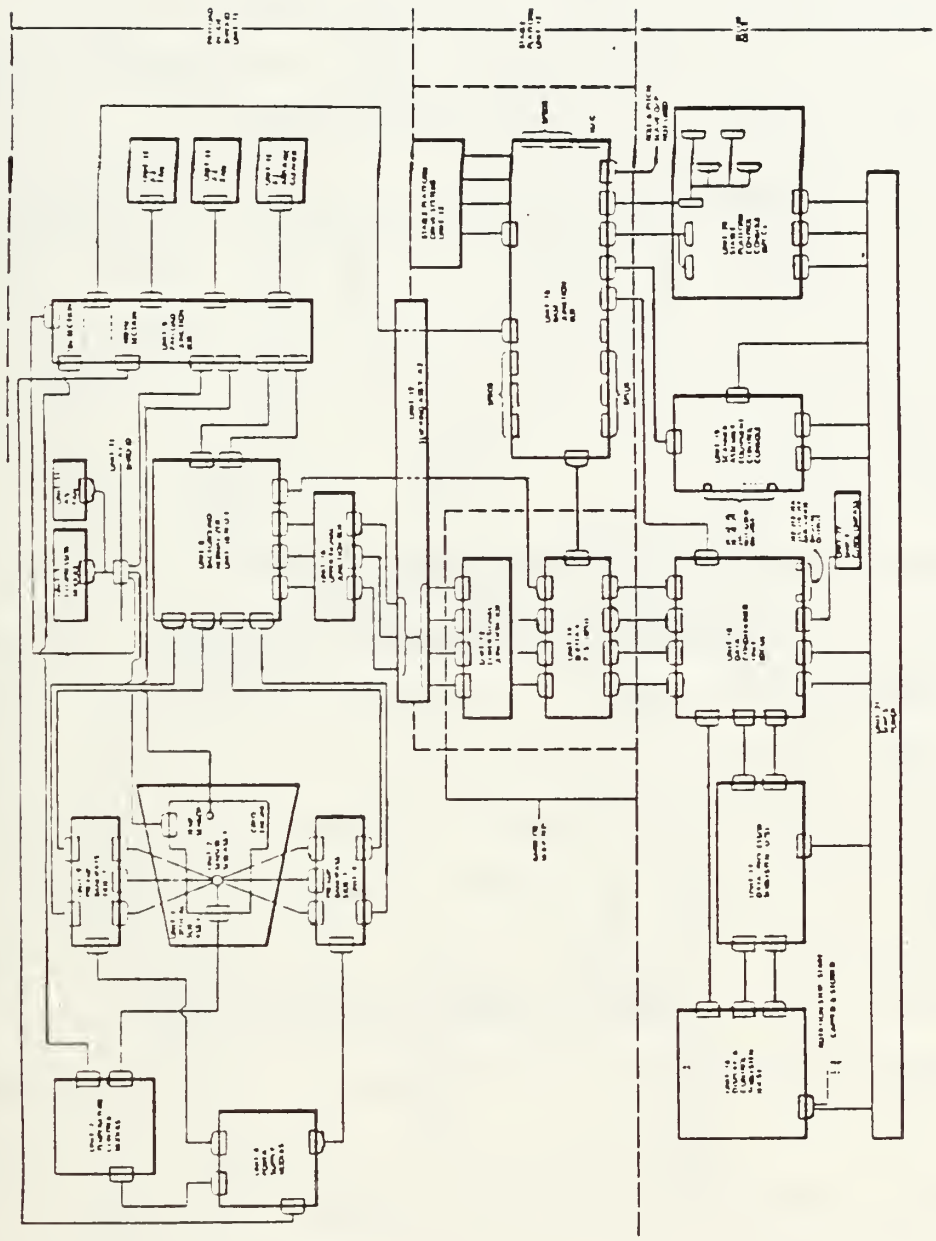

Figure 2. AN/SAR-8 Subsystem Block Diagram

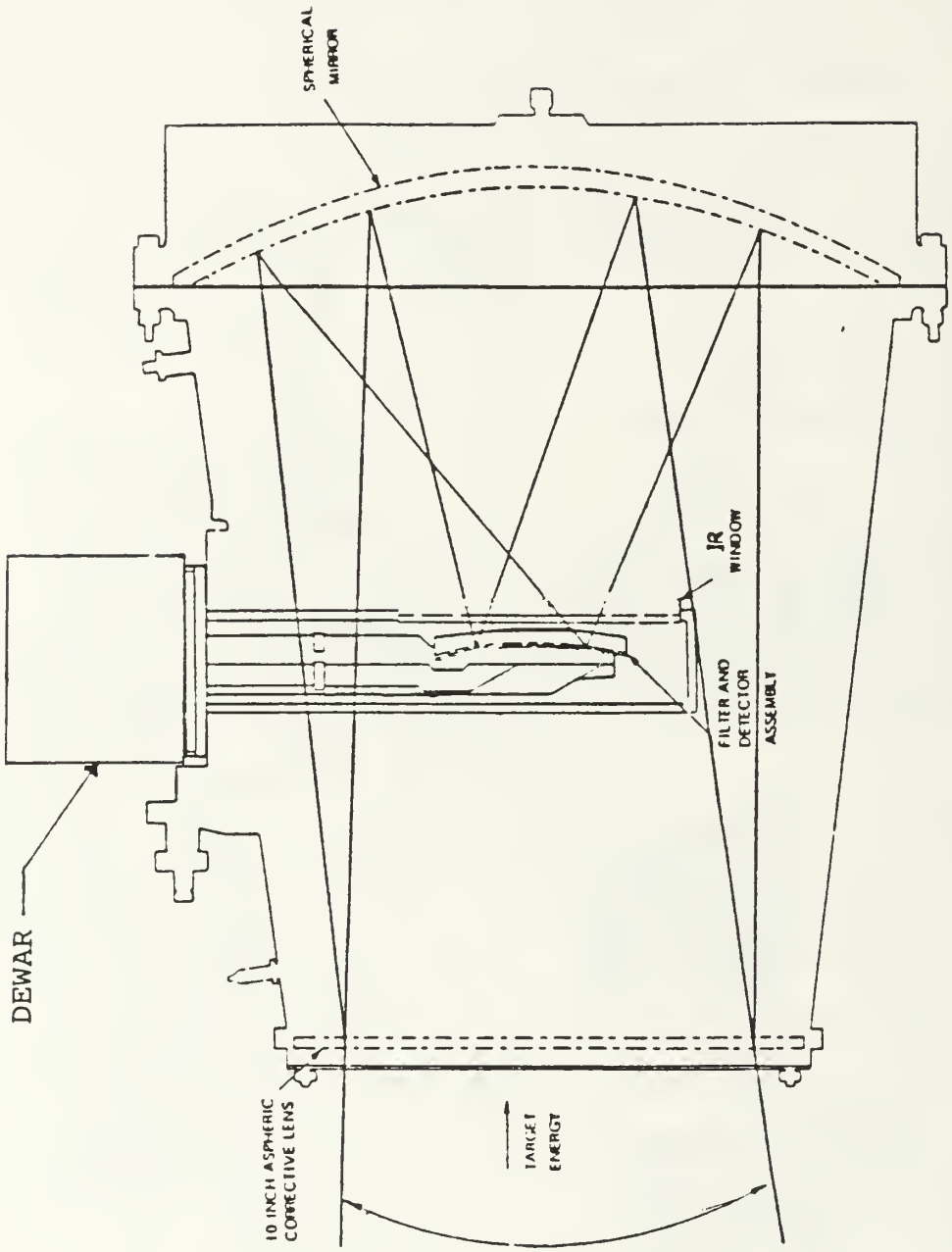

Figure 3. Optical Subassembly Diagram

window on the sensor probe. The germanium window was removed because of a change in the cooling system which will be discussed later.

The IR detectors consist of two vertical arrays of sensing elements in the focal plane of the Schmidt telescope. The telescope is rotated so as to sweep the image across the detector arrays. Each array incorporates a column of 90 indium antimonide photovoltaic linear detector elements. These two arrays are independent of each other and are covered by filters which pass selected wavebands of IR radiation in the 3 to 5 micrometer range. Each element has the angular dimensions of 2 x .3 milliradians with the larger being its height. Designated as the lead and the lag, these two arrays are separated by about one-half degree in azimuth. Each detector element is coupled to an electronic channel which carries the signal through the rest of the Scanner system. The detector array channels are connected to the Preamplifier-Bandpass Assemblies (PBA) through the Flat Conductor Cables (FCC). These FCCs use nickel conductors surrounded by nickel shields covered with a dielectric laminate material to reduce coupling to external electrical noise.

The IRSTD contains two PBAs which mount on the side of the optical housing. Each PBA unit serves 90 detector channels using 15 multilayer cards with 6 channels per card. The gain is different for each PBA unit. Side 1, serving the

lead array, has a voltage gain of 118 volts out per volt in. Side 2, operating on the lag array, has a voltage gain of 98 volts out per volt in. The input noise voltage at a typical 5 Kilohertz is 5 nanovolts per root Hertz. This yields a low PBA noise factor (detector noise / system noise) of 0.7 minimum.

The original cooling system was a double walled Dewar vacuum flask cooled by a cryogenic engine. This system was found to have irreparable damage and a decision was made to replace it with a simpler foam insulated design cooled with liquid nitrogen (LN) as seen in Figure 4.

Basically, liquid nitrogen is held in a reservoir above the detector cooling stalk. This well is a cylindrical chamber 3/4 inch in inside diameter and 6 inches long. The wall of the chamber is thin stainless steel. It is welded on the upper end to the 1/4 inch thick horizontal face plate which supports the detector structure. The plate is gasketed to the top surface of the outer wall of the telescope chamber. Since the upper end of the cooling stalk well must be at telescope wall temperature, it is necessary to provide cooling to the lower end of the stalk well without cooling the upper end of the stalk. This is accomplished by allowing the liquid nitrogen to flow into the cooling stalk well through a thin walled stainless steel feed tube that reaches deep into the cooling stalk and is separated from the inner wall surface of the cooling stalk by a thin layer of foam

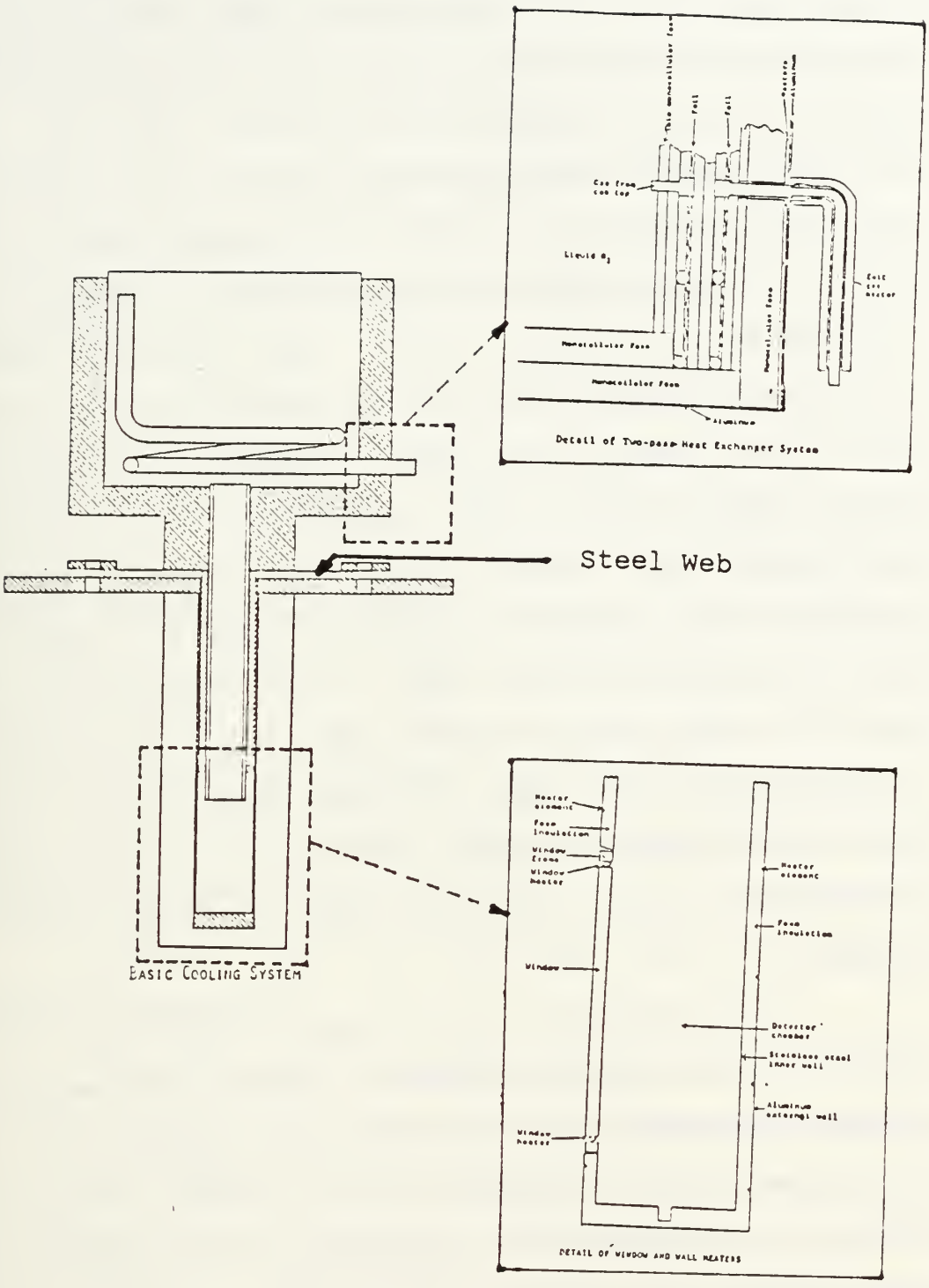

Figure 4. LN Cooling System

insulation. To prevent the liquid nitrogen from flowing out of the top of the cooling stalk well, the feed tube passes through and is soldered to a thin, .010 inch thick, horizontal web of stainless steel. This web is sealed at its outer edge to the 1/4 inch thick horizontal face plate with an O-ring. This allows the sealing O-ring to remain at room temperature at the outer edge of the stainless steel web. The web is separated from the face plate by the thickness of the O-ring. Since this space is sealed relative to the region outside the nitrogen chamber, no liquid resides in this space. Any initial liquid N_2 would evaporate and produce a back pressure preventing liquid from entering. To improve insulation in this gap, it also contains a layer of foam. The inner diameter of the feed tube from the reservoir to the cooling stalk well is large enough that liquid can flow down to the well freely and still allow for the passage of bubbles of gaseous nitrogen rising from the cooled well walls.

The evaporated dry nitrogen is used as a flushing gas for the telescope and detector chamber. The evaporating nitrogen is picked up at the top of the reservoir in two 1/4 inch copper tubing fittings. The gas is then led in plastic tubing down through the insulation in approximately four turns around the can in a layer at a distance one third of the way out through the insulation. The heat is spread in this layer with heavy aluminum foil. The tubing then makes

an additional pass to the top of the insulation at a distance two thirds of the way out through the insulation. This two-pass heat exchanger takes advantage of the heat capacity of the gas while warming it for use as a flushing gas. The hold-time of the reservoir is approximately doubled by the heat exchanger, and provides a hold time of approximately one hour.

The germanium infrared-transmitting window and the exterior of the detector head would become cold if left unheated during operation. This would be likely to cause degradation of the resolution of the telescope because of thermal convection within the telescope. It would also run the additional risk of dew or frost formation on the infrared window, in the event of poor drying of the atmosphere within the telescope. To avoid these problems, a heater is provided around the periphery of the infrared window, and a heated shield provided to cover the remainder of the detector head, to keep all these surfaces at telescope temperature.

The parts of the system external to the telescope are also heated to prevent problems that would otherwise occur from sweating of cold surfaces. The efflux gas used for flushing the detector head and the telescope interior is first warmed by circulation through the two-pass heat exchanger within the insulated walls of the reservoir and then heated further with two tubular external heaters.

A comparison between the temperature-versus-time cooldown curves of the mechanical refrigerator system and the new LN system is displayed in Appendix C.

2. Platform Subsystem

The Platform subsystem provides stabilization of the sensor subsystem and interface of IR data to other subsystems. It comprises equipment which rotates the scanner head and compensates for the ship's motion. Slip rings are contained which are used to transmit the filtered video output from the detector arrays to the processing equipment located belowdeck. The part of the platform which handled the ship motion adjustments was unnecessary for installation on a building roof and therefore was not included in the NPS IRSTD plans.

3. Scan Converter Subsystem

The Scan Converter reformats scan data for display presentation. Converters are available for processing multiple air and surface displays.

4. Electronic Processing Equipment

This provides for the signal processing as well as the data processing being carried out on the video output. The signal processor maintains filtering and normalization of the signals. The normalization can be carried out either with the hardware box mounted on the scanner head or by using software operating on the signal as it comes off the data tape. The data processor produces post-detection

processing including merging of detections, correlation with existing tracks, track initiation, track maintenance, target discrimination and target prioritization. It sends detection and track data to other shipboard systems for weapons control.

5. Display Subsystem

The Display Subsystem supplies the point of man-machine interface to the system. Operator inputs should include keyboard, function and target selection. It is through this subsystem that the operator observes and evaluates the end product of the data acquisition and processing performed by the AN/SAR-8. In integrated combat system applications the operator station may be eliminated from the system and its functions assumed by the combat direction computer or equivalent. At NPS a computer terminal will be set up to act as a display unit for stored data run through a processing program.

E. EDM IMPROVEMENTS

As a result of the extensive testing in the early years of the AN/SAR-8 program, several improvements have been incorporated in the current EDM which are not part of the NPS IRSTD system. These improvements are designed to increase the reliability and performance of the system.

An advanced detector array consisting of both InSb and HgCdTe elements is installed. This makes use of 3 to 5

micrometer radiation for detection and 8 to 12 micrometer radiation for thermal imaging.

New computer detect-and-track algorithms were created by General Electric, making use of new information gained about target data characteristics and background clutter. It is envisioned that further algorithm developments may be pursued using the modified ADM at NPS.

The use of fiber optics and rotary couplers in place of the current slip-rings and coaxial cable is to be integrated in the design of future shipboard IRSTDs within the next few years.

Lastly, the computers to be used in the EDM system have been upgraded to AN/UYK-44s which are much more capable computers than the old UYK-20s incorporated in the ADM IRSTD system.

III. EXPERIMENTAL PROCEDURES

A. GENERAL

Many items had to be completed prior to the calibration and initial operation of the IRSTD ADM here at NPS. The work leading to this thesis involved participation in the completion of the following system development tasks:

* Construction of a wooden base for the IRSTD scanner head, to facilitate movement of the scanner.
* The running and enclosure of cables leading from the control room to the roof.
* The transfer, drilling and installation of a heavy steel plate to act as a base plate for the crane installed on the roof for movement of the IRSTD scanner.
* The replacement of the steel base with the wooden base on the scanner head in order to reduce weight and facilitate movement in the control room.
* The relocation and drilling of the steel base to the roof stable platform.
* The building of removable guard rails on the roof to allow easy transfer of the scanner head with the crane.
* The cleaning of all mirrors, prisms, and lenses in the collimator.
* Installation of a 50 °C thermal cutout switch on the detector head to prevent accidental overheating of the germanium window.
* The re-positioning of the sensor subassembly inside the Optical housing on the scanner head, to compensate for removal of a germanium window.
* The placement of a 400 Hz power supply on the scanner head and the hookup of all leads.

These items along with various others were necessary in order to prepare the IRSTD for calibration and operation.

B. APPARATUS USED FOR CALIBRATION

The calibration equipment used in this experiment consisted of four major components: 1) the IRSTD scanner head, 2) the collimator, 3) a digital oscilloscope, and 4) a computer.

1. IRSTD Scanner Head

This equipment included the sensor subassembly discussed in Chapter One and the SPAR signal breakout box. The detector head was defocused so that a blur spot with a diameter of about 5 detector elements (10 milliradians) was created. This ensured that the center element was fully illuminated. The breakout box was organized into two sides with 90 connectors each. The input to the test box came from the Preamplifier-Bandpass Unit's output. A continuity check of the test box revealed that leads 3 and 6 on side 1 were open circuited. This problem was overcome by reversing the test box input cables and taking data for these two detector channels on the side 2 connectors whenever it became necessary.

2. Collimator

This device was used to produce a beam of parallel rays of radiation simulating an IR source at infinity. It incorporated a reflecting telescope with a 9 inch mirror, a

blackbody (BB) radiation source, and a chopper wheel as shown in Figure 5.

The telescope had a vernier dial that positioned a set of two wheels instead of an eyepiece. One wheel held a group of neutral density filters, not used in this calibration procedure. The other wheel included pinholes of various sizes along with a special disk (crosshair and circle) used for autocollimation. The focal length of the telescope was changed as the vernier dial was changed by a factor of 0.033 ± 0.001 inch per division.

The telescope was adjusted to focus at infinity by autocollimation. This involved putting a flat mirror, designed for this purpose, on the end of the mounting tube. A beam of light was reflected off a glass slide held at a 45 degree angle to the view tube of the telescope. This allowed the image marked on the disk, mentioned earlier, to be both illuminated and seen at the same time. The dial was then turned until the image was viewed without parallax. The vernier dial position was recorded as 040 which gave the focal length for the collimator of 135.9 ± 1.0 centimeters (cm).

The Blackbody source slides into position right behind the pinhole on the telescope. An IR-408 (serial no. 160) blackbody source was used with an IR-101 (serial no. 160) temperature controller both made by Infrared Industries,Inc. of Santa Barbara, California. They provided

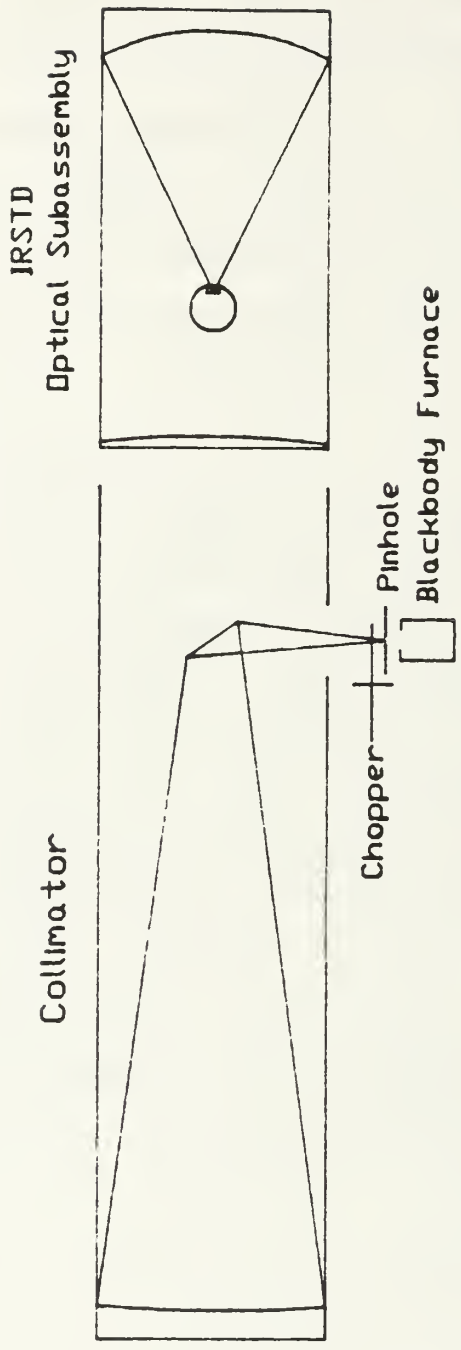

Figure 5. Collimator Diagram

a stable source of IR radiation of known flux and spectral distribution. The temperature controller supplied voltage at a rate of 0.041 millivolts per 1 °C at ambient room temperature within an accuracy of ± 3 °C. A setting of 20 millivolts was used thus maintaining a temperature of about 500 °C. An aluminum plate was drilled to provide an aperture of 2.56 ± 0.01 mm, and fitted onto the Blackbody to promote cleaner chopped signals.

A chopper assembly, consisting of an adjustable motor rotating a six inch wheel with 66 evenly spaced holes, was located in front of the pinhole. The speed of chopper wheel was set at 5.236 kilohertz to simulate the pulse produced by a point source seen by the telescope when the scanner head is rotated at its rated 30 RPM (1/2 revs/second). This frequency was determined using the following: 1) detector width is 0.3×10^{-3} radians, 2) one scan views π radians per second, 3) pulse width equals detector width divided by angle viewed per unit time, 4) the chopper period is twice the pulse width, and 5) the frequency equals to one divided by the period.

The collimator was placed horizontal on a table and raised onto two lab jacks. It was then lined up in front of the optical window of the scanner head with a set distance of 124.7 ± 1.0 centimeters from the telescope's parabolic collimating mirror to the IRSTD's 10 inch window. The lab jacks were used to change the elevation angle of the

collimator thereby placing the focal point on selected detector elements. It was determined that a change of 1/4 inch in height of the rear of the collimator was equivalent to a change of image location on the detector array of 2 milliradians (1 detector element). The front of the collimator was placed at the same height as the Scanner window's lower edge and was not raised in conjunction with the rear. After observing detector element responses over the entire range of elevation angles, the loss of incident radiation caused by this slight misalignment was determined to be negligible.

3. Digital Oscilloscope

The type of digital oscilloscope used was a Nicolet model 3091 (serial no. 86D03027).The Nicolet received data from the test box through an RG68 cable. This data was displayed as a single waveform of 4000 data points with a time per point setting of 1 microsecond. A waveform was obtained for each detector element, stored as data, and then sent via the Nicolet's RS-232 interface along a ribbon cable to the serial port of the data acquisition computer.

4. Computer

A Compaq Portable II computer was used to run the program which accepted data from the Nicolet and stored it as a data file on a hard disk. All of these data files were later transferred to the Masscomp computer maintained by NACIT for permanent storage and use as calibration data.

C. CALIBRATION PROCEDURE

The procedure itself was fairly simple. The blackbody source on the collimator flooded the reflecting telescope with incident IR radiation. This radiation came into the Scanner window as a set of parallel rays. The aspheric aluminum mirror focused the IR radiation onto the detector array of the sensor/probe subassembly. Each illuminated detector element generated a current which was sent to the Preamplifier-Bandpass Assembly Units. These units amplified this signal and sent it onto the channel breakout box. An RG68 cable carried the signal to the Nicolet oscilloscope where it was displayed as a waveform. The amplitude of the signal, measured from upper to lower peaks, was recorded and then the signal was sent via an RS-232 interface to the Compaq computer. The computer stored the waveform as a data file. Later, the average response for a detector channel for each preamp unit was computed by adding the amplitudes for a side and dividing by 90. Using this average value as the standard, the other detector channels were compared with it in order to determine their relative responsivities. An absolute calibration could not be performed because of the inability to measure incident radiation on the detector.

D. ROTATION SETUP

After the calibration data was taken, the IRSTD was set up to take data while rotating. This consisted of removing

the collimator table and hooking the slip ring cables up to the breakout box. These cables allowed data to be taken from the Buffer Power Unit (BPU). The breakout box was secured to the scanner head and the N_2 purging lines were connected to the dewar vent lines. A glowbar was placed at a distance of 15.3 meters from the scanner window. Using the NPS IRSTD's new capability, the detector array was focused at this distance by sliding the sensor/probe subassembly forward approximately 5 millimeters from the milled shoulder on top of the optical subassembly. A sheet of paper was placed over the upper 3/4 of the scanner window in order to reduce the size of the signal. The Nicolet's external trigger was connected to the scanner's optical rotation indicator. The time per scan was adjusted so that only that period of time the scanner was looking at desired targets would be displayed on the Nicolet. These details made the IRSTD ready for rotation.

E. PROBLEMS ENCOUNTERED

Several problems of varying magnitudes were experienced during the calibration of the IRSTD. Two of these problems are worthy of discussion.

Several detector channels did not give signals out as expected. The cause of this could have been in the detector elements, the FCCs, the PBAs, or the BNC connectors. All

were checked for bad channels. Some improvement occurred when the FCCs were tightened down.

The largest problem encountered was a shadow pattern caused by the detector head being in the defocused position. This pattern consisted of the blur spot image and a region of darkness as shown in Figure 6. The dark region was determined to be the shadow of the sensor/probe subassembly which was being imaged onto the detectors. This problem was overcome by measuring the response peak observed to one side of the shadow region. The lead peak was chosen in all cases to ensure repeatability of results.

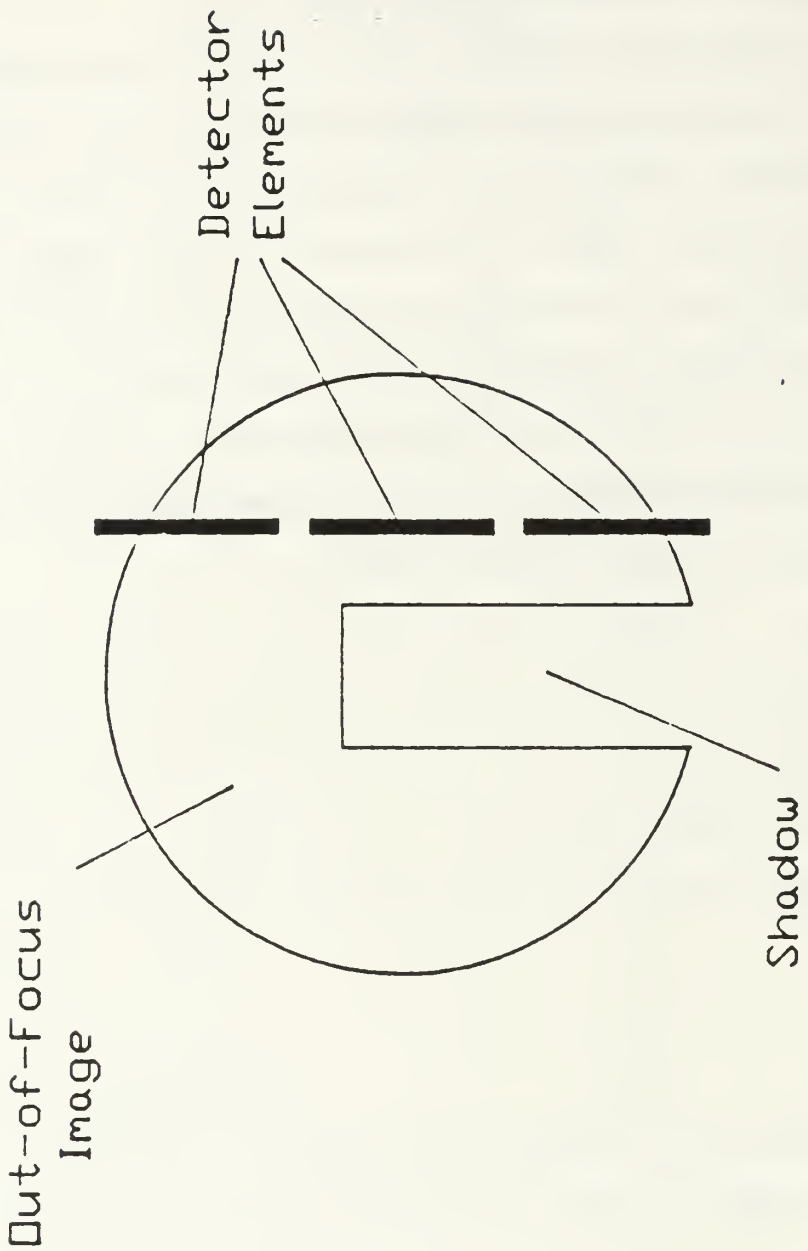

Figure 6. Defocused Blur Spot With Shadow

IV. RESULTS

This section summarizes the major results of this investigation. In describing the results, detector elements using the designation 100 will be those on side 1, the lead array. The designation 200 will characterize those elements on side 2, the lag array. From the waveforms displayed on the Nicolet screen, amplitudes were taken which represent the difference between the maximum and minimum signal peaks as shown in Figure 7. These amplitudes were used to determine the relative responsivity between the detectors on a specified side. The disparity between the lead and lag array occurs because they use different optical bandwidth filters. These filters pass only that radiation with wavelengths in a specified band. Thus the lead and lag array detector elements receive incident radiation of different frequencies. The amplitudes are given in the voltage output of the Preamplifier-Bandpass Assemblies rather than the current generated in the photovoltaic detector elements. The temperature of the detector elements was maintained at 86 K during the period of data taking.

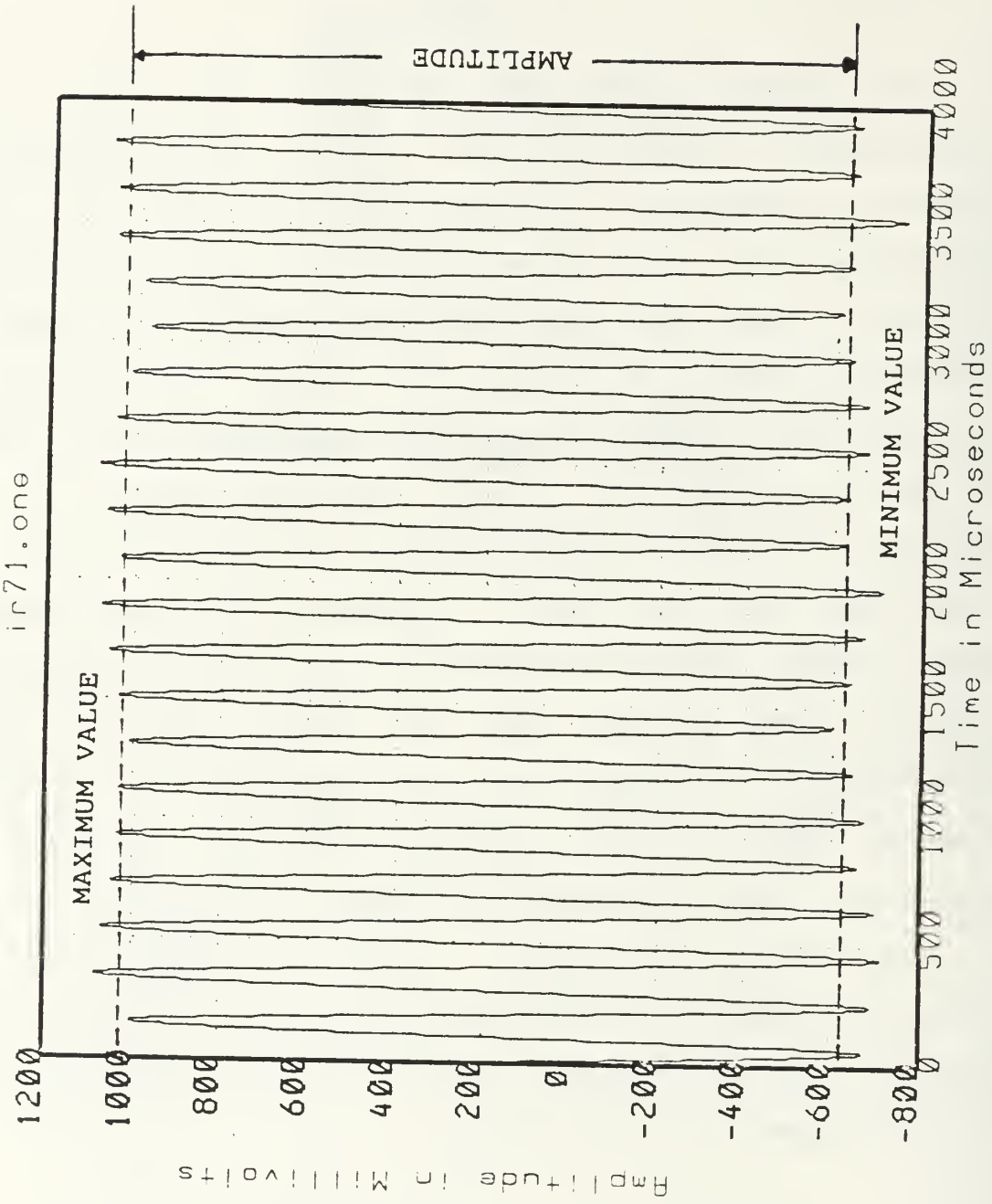

Figure 7. Sample Amplitude Measurements

A. CALIBRATION DATA

This data was generated from the procedure explained in the previous section. Table I lists the results of the measurements that were taken.

TABLE I

RELATIVE RESPONSIVITY RESULTS

	Side 1	Amplitude (volts)		Side 2	Amplitude (volts)
	101	1.522	*	201	0.020
	102	1.350		202	3.433
	103	1.580		203	3.382
	104	1.904		204	3.189
	105	1.900		205	3.512
	106	1.747		206	3.400
	107	1.681		207	3.261
*	108	0.071		208	3.321
	109	1.651		209	3.302
	110	1.622		210	3.163
	111	1.762		211	3.132
	112	1.631		212	3.320
	113	1.583		213	3.251
	114	1.790		214	3.189
*	115	0.400		215	3.180
	116	1.751		216	3.166
	117	1.838		217	3.262
	118	1.782		218	3.305
	119	1.702		219	3.391
	120	1.691		220	3.119
	121	1.750		221	2.802
	122	1.763		222	3.028
	123	1.612		223	3.202
	124	1.791		224	3.270
	125	1.643		225	3.140
	126	1.592	*	226	0.020
	127	1.642	*	227	0.022
	128	1.661	*	228	0.600
	129	1.581	*	229	0.600
*	130	0.050	*	230	0.030
	131	1.611	*	231	3.050
	132	1.692		232	2.475
	133	1.702		233	3.050
	134	1.722		234	3.000
	135	1.800		235	3.322
	136	1.830		236	3.120
	137	1.650		237	3.122
	138	1.381		238	3.030

TABLE I
(Cont)

	139	1.680		239	3.150
	140	1.740		240	3.361
	141	1.604		241	3.281
	142	1.730		242	3.410
	143	1.756		243	3.450
	144	1.712		244	3.452
	145	1.693		245	3.404
	146	1.831		246	3.303
	147	1.840		247	3.233
	148	1.811		248	3.261
	149	1.811		249	3.383
*	150	0.030	*	250	1.183
	151	1.665		251	3.291
	152	1.699		252	3.268
	153	1.794		253	3.113
	154	1.835		254	3.201
	155	1.791		255	3.242
	156	1.712		256	3.144
	157	1.729		257	3.109
	158	1.702		258	3.280
	159	1.791		259	3.131
	160	1.729		260	3.231
	161	1.690		261	3.058
	162	1.679		262	2.911
	163	1.673		263	3.102
	164	1.790		264	3.055
	165	1.742		265	3.141
	166	1.819		266	3.031
	167	1.668		267	3.101
	168	1.733		268	3.149
	169	1.820		269	3.267
	170	1.720		270	3.110
	171	1.770	*	271	0.015
	172	1.592		272	3.340
	173	1.824		273	3.299
	174	1.833		274	3.219
*	175	0.035		275	3.160
*	176	0.030		276	3.042
	177	1.829		277	3.164
*	178	0.030	*	278	2.613
	179	1.902	*	279	2.580
	180	1.870	*	280	2.480
	181	1.876		281	3.142
	182	1.854		282	2.970
	183	1.704		283	2.882
	184	1.621		284	3.082
	185	1.711		285	3.213
	186	1.751		286	3.330
	187	1.662		287	3.161

TABLE I
(Cont)

188	1.662	288	2.952
189	1.640	289	2.840
190	1.681	290	2.919

* Denotes that the detector channel's response is irregular.

Mean values for the amplitude of the detector outputs were worked out for each side using the following statistical analysis [Ref. 4]:

$$\langle x \rangle = (x_1 + x_2 + \ldots + x_n) / (n)$$

$$s = \left(\Sigma_{i=1}^{n} (x_i - \langle x \rangle)^2 / (n-1) \right)^{1/2}$$

where $\langle x \rangle$ = population mean

n = sample size

s = population standard deviation

One standard deviation was used as the estimated error for these values.

$$\langle x \rangle_{Side1} = 1.719 \pm 0.102 \text{ volts}$$

$$\langle x \rangle_{Side2} = 3.184 \pm 0.158 \text{ volts}$$

Thus the standard detector for the lead and lag arrays would have these corresponding amplitudes. Graphs for all of the detector elements which were considered not up to these standards are displayed in Appendix B. The Noise Equivalent Power of this standard detector should be similar to the

value of 2.5 x 10^{-11} Watts found in a commercial InSb detector operating at 77 K with a 500 K source [Ref. 5]. Using this standard value, D* was determined to be approximately 8.0 x 10^{10} (cm $Hz^{1/2}$ / Watt).

B. ROTATING DATA

The next step after taking static calibration data was to take data with the sensor head rotating. This was accomplished subsequent to the changes in set up as explained in Section III. The scans look very different from the static case in that the collimated chopped signals were replaced by single peaks representing point sources. A total of 30 scans were taken using various detectors at different elevation angles. These waveforms were also sent from the Nicolet to be stored as data files, which were plotted out and examined. The plots revealed that the sensor assembly was functioning properly, with the glowbar and other hot points being prominently displayed. The noise levels acquired between targets were caused by background radiation which exceeded the threshold of the detector elements. Appendix D compares one of the rotating IR plots with a visual photograph of the same scene.

C. ERROR ESTIMATION

Every effort was expended to ensure that the hundreds of measurements taken and data files stored were a true

representation of this system's response to IR sources. In spite of this care, the low levels of voltage requiring considerable amplification and the intricacy of the equipment did generate some areas where error could occur.

Systematic errors are those due to imperfections in the design of the experiment or in the measuring instruments. These errors are hard to detect. Cross checks were made often on the data collected to make sure that it was correct. The environment around the scanner head and the calibrational equipment was controlled as much as a closed room would allow.

Random errors are the statistically fluctuating differences between instrument readings and the average value of many such readings all taken under identical circumstances. These errors which usually affect the reproducibility of the data were found to be of small magnitude (less than 5 %) when verification was carried out. The variation of the collimator's Blackbody source could account for some differences in measurements; however, this should be a small amount as the source was rated ± 3 °C at stabilized temperature.

V. CONCLUSIONS AND RECOMMENDATIONS

A. CONCLUSIONS

The Installation of the Modified AN/SAR-8 ADM at NPS will be an important step forward in the evolution of the AN/SAR-8. This system will enable NPS to gather uncompromised background data, which up to this point has not been done. This data can be recorded and altered for the testing of processing algorithms and new equipment.

The NPS IRSTD has a much better temperature-versus-time cooldown curve than the original ADM as can be seen in Appendix C. It reaches an operational temperature of 90 K within 9 minutes as compared to over 45 minutes with the old system. The InSb detectors were observed to become noisy as their temperature increased above 130 K. The detectivity started to deteriorate at 134 K with total loss of signal for temperatures above 138 K. The equilibrium operating temperature for the detectors of the LN system is 85 K compared to 82 K for the cryogenic engine. One disadvantage of the LN dewar is that it only allows an operational time of approximately 55 minutes before it needs refilling.

The calibration data revealed which detector channels were not operating within the prescribed standards. These channels are disclosed in Table II.

It is important to remember that a defective channel does not imply that the detector element is impaired. The reason could be in the wiring, the FCC cables, or in the PBA card for that element.

TABLE II

LIST OF DEFECTIVE DETECTOR CHANNELS

Lag Array	Lead Array
01	08
26	15
27	30
28	50
29	75
30	76
50	78
71	
* 78	
* 79	
* 80	

* Denotes that detector is operational but signal strength is significantly diminished.

These defective channels presented a real problem in the compiling of data. Some channels displayed marked improvement when the FCC cables which connect the sensor/probe subassembly to the PBAs were flexed and tightened. The nonfunctional channels number 15 out of a total of 180. This represents 8.3% of the detector channels and is less than the system's replace-or-repair requirements of 10% [Ref. 6]. Special notice should be given to the fact that both the lead and lag arrays have defective channels covering the same elevation angle in two instances, 30 and 50. This could lead to difficulties detecting and tracking targets that pass through these elevation angles when the IRSTD is fully

operational. An example of the way these defective channels appeared on testing trials prior to coming to NPS is shown in Figure 8 [Ref. 7]. Note that some detectors previously reported defective are now active.

Another problem occurs with the Pre-amplifier Bandpass cards. They have a MTBF (mean time before failures) design goal of 1000 hours [Ref. 6]. It can be assumed that all of these cards will exceed this time period within the first two years of full operation at NPS. Circuit boards of this kind, however, generally show very low failure rates after burning. Since they are also custom cards, the expense of procuring spares does not seem to be justified. In the event of failure an "ad hoc" solution to the problem should be sought. This approach is valid in the academic environment though not in the operational world.

This study has demonstrated that a relative responsivity value can be determined even when the incident radiation input or voltage output per detector is unknown. The average detector response for a collimated IR source produced by a Blackbody at 500 °C was determined for both the lead and the lag array. Comparison of their relative amplitudes reveals that the lag array maintained a factor of 1.85 improvement over the lead array for the same IR source at 500 °C. This improvement was determined to be caused by the use of different bandwidth filters for the two arrays.

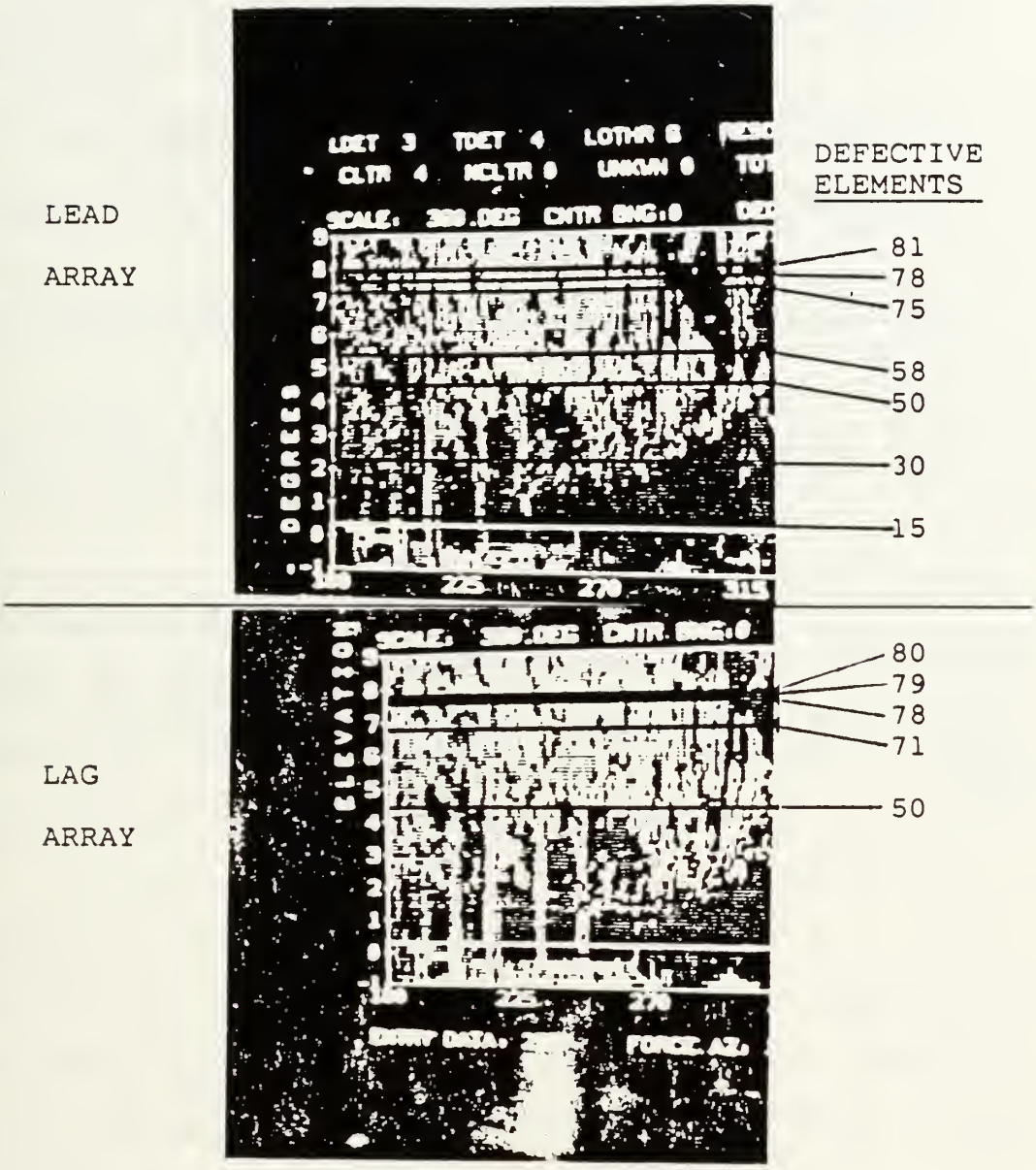

Figure 8. Raw Video With Defective Scan Lines

B. RECOMMENDATIONS

The following recommendations are made:

* When the data processing link to the Masscomp is completed, perform comparison checks on the data with that coming out of the amplifiers in the control room.

* Disconnect and then reconnect the FCC cables in order to see if any detector channels can be recovered.

* Keep the collimator operational so that data checks can be made whenever uncertainties arise.

* Research the methodology and requirements of replacing the detector array with detector elements of the latest Focal Plane Array type.

* Have a foam cover sunshade made for the scanner window that will help prevent direct incident solar radiation when the sun is at certain elevation angles.

It is hoped that these recommendations will be acted upon by the appropriate personnel at NACIT in order to further the operational life and capabilities of the NPS IRSTD.

APPENDIX A

INFRARED THEORY

A. GENERAL

Unlike the ultraviolet and visible regions of energy absorption and emission for gaseous media, associated with changes in the electronic configuration of atoms, infrared radiation from a solid source is generated by the molecular thermal action within an object. Thus any object at a temperature above absolute zero has atoms that are continuously oscillating or rotating about equilibrium positions within the molecular framework. These movements cause IR emission and absorption to occur, provided that changes of electric dipole moment are involved. Vibrational effects are usually responsible for emission and absorption spectra in the shorter wavelength portions of the IR region (to ~ 30 μm). Pure rotational effects usually lead to emission or absorption in the far IR region (i.e. > 100 μm). These effects are often superimposed, and the complexity of the spectra depends upon whether the vibrational effects are harmonic or mechanically or electrically anharmonic and upon the spacing of superimposed rotational effects.

The Infrared region of the electromagnetic spectrum is commonly agreed to be located between 0.75 and 1000

micrometers (μm or 10^{-6} meters). The IR region is subdivided into four bands as shown in Table III.

TABLE III

INFRARED REGION

BAND	WAVELENGTH (μm)
Near Infrared	0.75 to 3
Middle Infrared	3 to 6
Far Infrared	6 to 15
Extreme Infrared	15 to 1000

Since the wavelength of IR radiation lies between the visible and microwave regions as shown in Figure 9, it has some characteristics of both [Ref. 8]. The IR can be focused or directed by the use of optical lenses and at the same time can be transmitted (like microwaves) through some materials which are opaque to optical light waves. The limited optical transmittance of common materials imposes special problems in the study of IR phenomena. Glass prisms and lenses are almost useless beyond wavelengths of about 3 micrometers. Various alkali halides are suitable for transmission of IR only to wavelengths of approximately 28 micrometers. Gratings are required as dispersing devices at longer wavelengths. Fortunately, the reflectivity of some mirror surfaces increases as wavelength increases. Gold or silver deposits on glass are excellent for the redirection of infrared rays. Because the material refractive index is high, aberrations and astigmatism effects are usually very small within infrared systems.

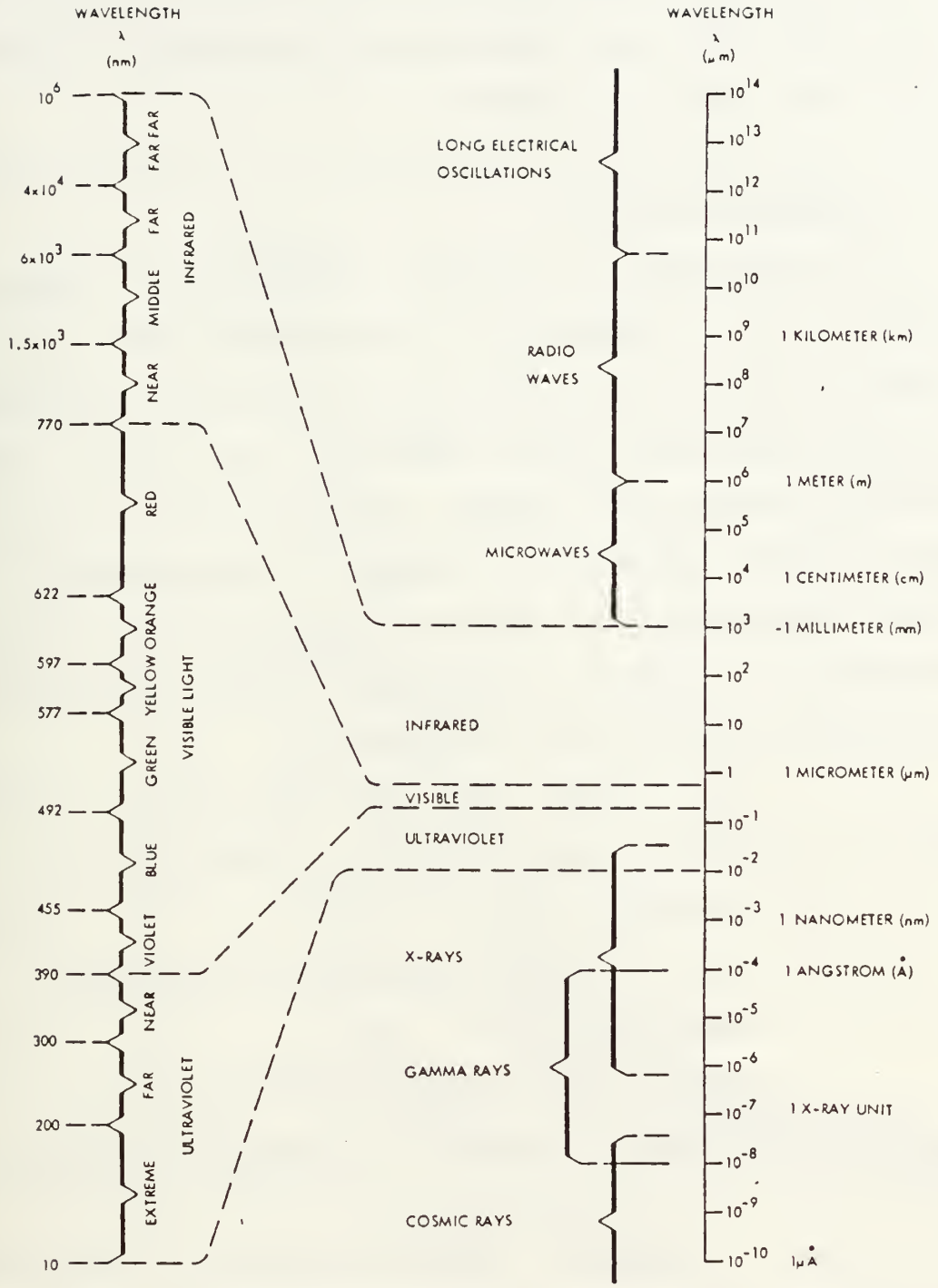

Figure 9. Electromagnetic Spectrum

This thesis deals mainly with the middle infrared region as the NPS IRSTD uses Indium Antimonide detector elements to detect and track air targets.

B. BLACKBODY RADIATION

To understand IR radiation emitted from a real world source, it is necessary to understand the theory of radiation from an ideal source. A blackbody represents a limiting case never quite reached by an actual body. A blackbody absorbs all thermal radiation striking it and is also a perfect radiator. It radiates at all wavelengths, and at any temperature its spectral radiant emittance reaches a maximum for a specific wavelength. Planck's law gives the spectral distribution of a blackbody as:

$$W_\lambda = (2\pi hc^2 / \lambda^5) \cdot (e^{ch/\lambda kT} - 1)^{-1}$$

where W_λ = spectral radiant emittance (Watt cm^{-2} μm^{-1})

λ = wavelength (m)

h = Planck's constant (6.6256×10^{-34} Watt sec^2)

T = temperature (K)

c = speed of light (2.9979×10^8 m sec^{-1})

k = Boltzmann's constant (1.3805×10^{-23} Watt sec K^{-1})

A graph of spectral radiant emittance as a function of wavelength is shown for a range of temperatures from 500 to 900 K as Figure 10 [Ref. 5]. The dotted line, which connects the maximum spectral radiant emittances, is a plot of Wien's

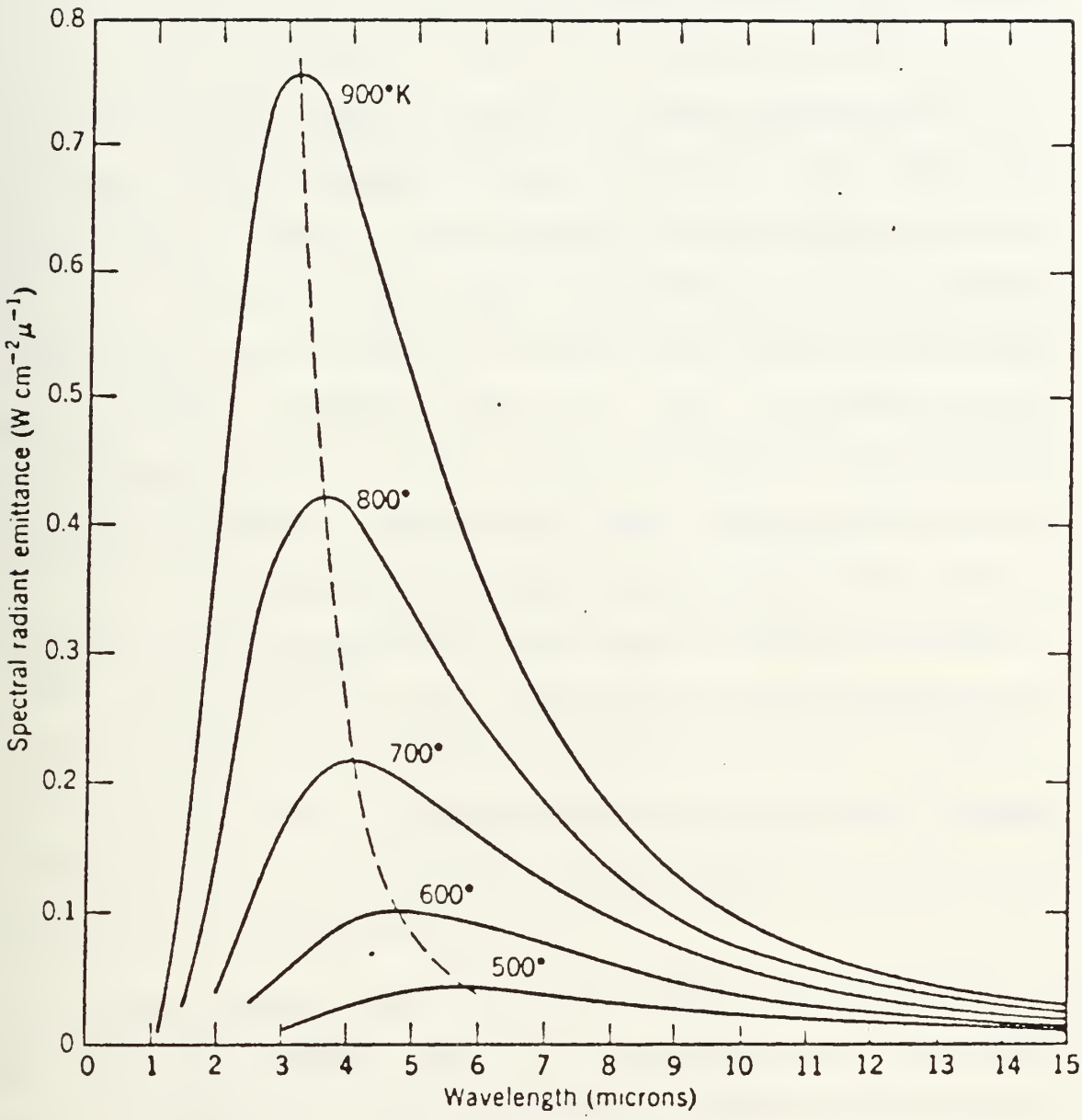

Figure 10. Spectral Radiant Emittance

displacement law which can be obtained by differentiating Planck's formula with respect to λ:

$$\lambda_{max} \cdot T = 2897.8 \ \mu m \ K$$

where λ_{max} = wavelength (μm)

This equation, for a specific temperature, gives the wavelength at which the maximum spectral radiant emittance occurs. It may also be applied in reverse. Given a peak wavelength the temperature can be calculated. At room temperature (300 K) the peak of radiant emittance lies at 9.7 micrometers, in the far infrared; while at the temperature of liquid nitrogen (77 K) the maximum of the almost insignificant amount of radiant emittance occurs at 38 micrometers, in the extreme IR wavelengths.

By integrating Planck's law with respect to λ, we obtain the total radiant emittance (W_b) of a blackbody:

$$W_b = \sigma \cdot T^4$$

where σ = Stefan-Boltzmann constant

$\sigma = 5.7 \times 10^8$ (Watt m^{-2})

This formula states that the total emissive power of a blackbody is proportional to the fourth power of its absolute temperature. This is equivalent to finding the area under the spectral emittance curve. Thus, the hotter an object is, the more energy it emits in the IR region. The energy emitted by a thermal radiator is not transferred as a

continuous flow but occurs as discrete energy packets called photons.

The previous discussions and equations apply to a blackbody radiator. By modifying the equations with a factor that varies according to the source, these equations can be made applicable to greybodies. Greybodies are objects which have a radiation efficiency of less than 100%. The correction factor is called emissivity. Emissivity is the ratio of the radiant emittance of a greybody to the radiant emittance of a blackbody at the same temperature, therefore, it is always a number between 0 and 1. Objects with a constant emissivity such as heated metal parts, personnel and environmental backgrounds can be approximated as greybody emitters. Objects which have an emissivity that is a function of wavelength are called selective radiators. They form a militarily important body of emitters (i.e. rocket plumes, jet exhausts and combustion engine exhausts). Selective radiators radiate energy in very discrete spectral intervals which are specified by the material's constituent properties and characteristics.

C. RADIATION SOURCES

A background source, either natural or artificial, is the emitter of IR radiation from the environment surrounding the target to be detected. It encompasses landscapes, the ocean surface, sun, clouds or blue sky. In order to prevent

the target's being masked out by the background, an IR system must be able to discriminate between the energy received from the two sources. Military air targets generally exhibit three types of IR radiation sources which can be differentiated from the background: aerodynamic heating, hot metal parts and exhaust plumes.

The aerodynamic heating of the skin of a plane occurs when it pushes the atmosphere out of its path. The final temperature generated is dependent upon the plane's shape and speed, generally reaching about 550 K. Aerodynamic heating leads to an emission whose peak is around 5 micrometers and can be modeled as a greybody for calculation purposes. The emissions which result from aerodynamic heating are important because they appear when the target is approaching the sensor and thus the exhaust pipe and plume could be obscured by the body of the target. [Ref. 9]

The hot metal tailpipe is a cylindrical cavity heated by the engine exhaust gases and is often equal to these gases in temperature. This temperature varies widely depending upon the type of engine used, from 290 °C for a turbofan to 4500 °C for a rocket. Hudson [Ref. 8] states that, for engineering purposes, the tailpipe has an effective emissivity of 0.9 and may be modeled as a greybody.

Another IR source occurs when the exhaust gases expand and mix with the atmosphere immediately upon leaving the tailpipe. The result is that the plume temperature decreases

rapidly with an increase in distance from the tailpipe. Carbon dioxide and water vapor compose the largest portion of the exhaust plume. These yield a spectral distribution with spikes in the radiance as a function of the wavelength (i.e. a selective radiator).

D. ATMOSPHERIC PROPAGATION

The atmosphere consists of a mixture of gases, mainly nitrogen, oxygen, carbon dioxide and water vapor, and aerosols, such as haze, fog, dust, and rain. The gas molecules and aerosol particles cause extinction of the radiation through the processes of scattering and absorption. Scattering is the process by which a particle in the path of an electromagnetic wave continuously 1) extracts energy from the incident wave and 2) reradiates that energy into the solid angle centered at the particle. The process can be explained in terms of electromagnetic wave theory. Briefly, the electric field of the incident or primary wave sets into oscillation the electric charges of the particle, be it a cloud droplet or molecule. The oscillating charges constitute one or more electric dipoles which radiate secondary spherical waves. These secondary waves bear a fixed phase relation to the primary waves. Scattering is a continuous process and when averaged over complete cycles produces no net change in the internal energy states of the particles. Spectrally, the process is also continuous, but

is strongly dependent on wavelength for a given particle size.

While scattering produces no net change in the internal energy states of the particles, absorption causes such a change and requires quantum theory for its explanation. In a molecule, the internal energy is partitioned into rotational, vibrational, electronic and translational energy, with the first three quantized to discrete levels. The incident radiant energy is absorbed as a quantum and the molecule undergoes a transition from a lower to a higher state of one of the three quantized internal energy forms. If, before the molecule can relax to the ground state and re-emit, molecular collisions occur, then non-radiating transitions can take place. In the case of thermodynamic equilibrium the energy is shared equally among all accessible internal energy states. When part of the energy is transferred to translational or kinetic energy, the process is called absorption. This energy therefore causes a heating of the atmosphere and the subsequent output of IR radiation.

The absorption in the atmosphere, mainly by carbon dioxide and water molecules is so great at certain frequencies that the atmosphere is practically opaque. Figure 11 [Ref. 8] shows a typical plot of the transmittance of the atmosphere versus wavelength. From this plot, it can easily be seen why the three transmission bands or "windows"

from 0.5 to 1.06 micrometers, 3.0 to 5.0 micrometers and 8.0 to 14.0 micrometers have been used in visible and infrared systems.

Atmospheric transmittance, the ratio of the decreased radiant intensity due to absorption and scattering losses to the incident radiant intensity, is a function of wavelength, path length, pressure, temperature, humidity, and the composition of the atmosphere. An equation for atmospheric transmittance, only valid for narrow wavelength bands with a constant linear extinction coefficient enclosed in an atmosphere of uniform composition, is given by:

$$T_a = e^{-\mu R}$$

where T_a = atmospheric transmittance

μ = linear extinction coefficient (km^{-1})

R = path length (km)

The extinction coefficient in the above equation is the sum of the coefficients for total absorption and for total non-forward scattering as given by:

$$\mu = \sigma_{ab} + \sigma_{sc}$$

where σ_{ab} = total absorption coefficient

σ_{sc} = total scattering coefficient

Both the scattering and absorption coefficients can be divided into components due to the molecules of the air and the aerosol particles suspended in it; i.e.

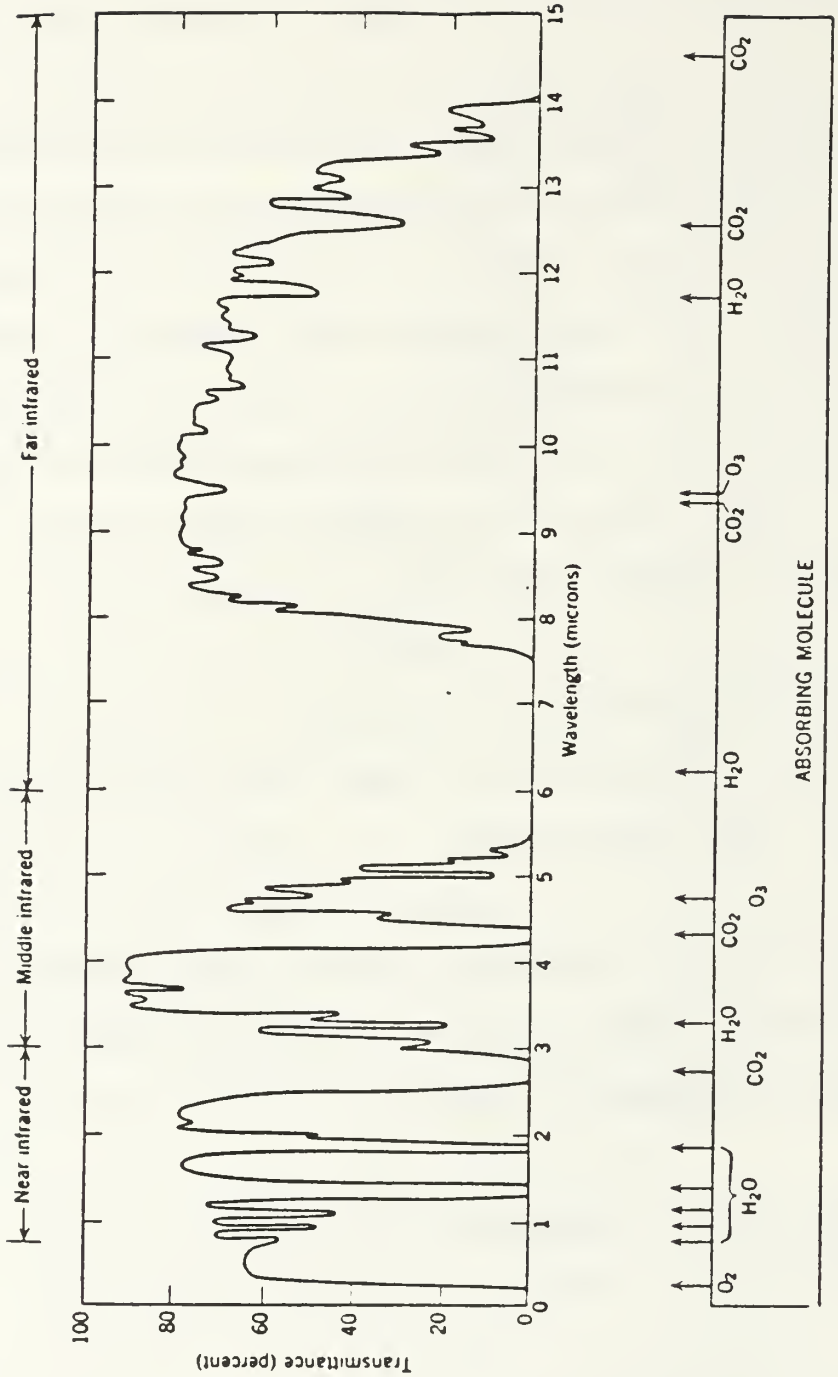

Figure 11. Atmospheric Transmittance

$$\sigma_{ab} = k_m + k_a$$

$$\sigma_{sc} = \sigma_m + \sigma_a$$

where k_m = molecular absorption coefficient

k_a = aerosol absorption coefficient

σ_m = molecular scattering coefficient

σ_a = aerosol scattering coefficient

The relative values of the four coefficients depend strongly on the density and molecular composition of the atmosphere and the composition, number density and size distribution of the aerosols. In the IR region, the absorption process is a greater problem than the scattering process due to the wavelengths (particularly 8 to 14 μm) involved and the concentration of the absorbing molecules.

E. INFRARED DETECTORS

The purpose of the detector element is to take the incoming infrared energy and produce an output voltage which can be amplified and processed by the electronic processing equipment. The detector selected for a particular system is chosen so as to ensure that the peak responsivity is within the spectral range of the expected targets. The detectivity should also be linear within the same spectral region.

There are two principal types of detectors: thermal and photon. Thermal detectors utilize the temperature increase produced in an absorbing receiver. The main disadvantage of

thermal detectors is their comparatively slow response to radiation changes. Photon detectors are made of semiconductor material in which the transfer of electrons is directly associated with photon absorption. This is the type of detector used in the IRSTD.

The photon's energy is inversely proportional to the wavelength associated with it. There is a "cut-off" wavelength beyond which the energy of the photon is insufficient to lift an electron across the bandgap of the semiconductor material.

There are two principal types of photon detector of interest; photoconductive and photovoltaic. In a photoconductive detector the conduction electrons and holes increase the detector's conductivity. For the photovoltaic detector the radiation-generated charge-carriers are swept away by the electric field in a p-n junction, thereby directly producing a current (voltage in open-circuit conditions) rather than a change in conductivity. The detectors in the NPS IRSTD operate in the photovoltaic mode.

The fact that photon detectors are sensitive, and have a shorter response time than other types, is an advantage where high-speed scanning is involved. A drawback is the fact that they must be cooled to achieve optimum sensitivity, usually around the temperature of liquid nitrogen. The InSb detectors used in the NPS IRSTD have a wavelength-response limited to wavelengths shorter than 5.5

micrometers operating at a temperature of 85 K. This limit in spectral-response is more than compensated for by the increase in sensitivity of the InSb detector within the 3 to 5 micrometer range as opposed to the other detectors for this band.

A widely accepted figure of merit for expressing the sensitivity of IR detectors is a quantity called the 'specific detectivity'. The symbol for specific detectivity is D* (pronounced "dee-star") and it is given by:

$$D^* = (A_d \cdot df)^{1/2} / NEP$$

where A_d = the detector area

df = the electrical bandwidth of the electronics

NEP = Noise Equivalent Power
(Input power needed to give a Signal/Noise = 1)

D* is a normalized figure of merit that is particularly convenient for comparing the performance of detectors having different system electronic bandwidths. D* assumes higher values for "better" detectors.

In the case of an ideal thermal detector which has a perfectly flat spectral response curve, it is sufficient to state a single value of detectivity. However, the situation is more complicated with photon detectors, whose spectral response is not flat, and typically drops off to zero at the long-wavelength cut-off point. The D* is, then, wavelength dependent and consequently bears the usual subscript, D^*_λ, whose maximum is at the peak of the spectral response curve.

The ultimate limit on detectivity is set by the 'radiation noise' signal which is generated in a detector, resulting from the statistical fluctuation of the radiation received and re-emitted by the detector itself. The noise signal is characterized by its random fluctuations in amplitude, frequency and phase. A detector in which this noise sets the limit of detectivity is said to be 'background limited'. This background limitation constitutes the optimal situation, since all system generated noise is reduced to negligible amounts.

The following parameters are used when one measures the properties of infrared detectors or interprets data measured by others: 1) the IR incident on the detector, 2) the electrical output of the detector, 3) geometrical properties of the detector, 4) the detector as a circuit element,and 5) the detector temperature. Without all of these parameters an absolute determination of the properties cannot be made.

APPENDIX B

GRAPHS OF DETECTOR RESPONSES

These graphs were made from the data files stored on the Masscomp computer maintained by NACIT. They represent the detectors' response to the chopped incident collimated radiation put out by a Blackbody at 500 °C. The chopping frequency was sustained at 5.236 kilohertz. Each data curve is a graph of amplitude-versus-time with the amplitude in millivolts and the time in microseconds.

The designation for which detector is being shown is placed above the graph. It is displayed as three parts. The first is the data set identifier, IR. The second is the detector number, ##. The third represents which array it is from, one for lead and two for lag. An envelope oscillation was observed on both lead and lag signal waveforms. This oscillation was determined to be caused by the 400 Hz power supply.

The impaired responses are grouped in three different types. A low noise signal ($\leq$ 80 millivolts) is displayed on the lead array (detectors 8, 30, 50, 75, 76, and 78) and on the lag array (detectors 1, 26, 27, 30, and 71). A periodic noise ($\sim$ 450 millivolts) also exists on both the lead Array (detector 15) and the lag array (detectors 28,29, and 50).

Three detectors (78, 79, and 80) on the lag array exhibit a reduction in signal amplitude of about 75 %.

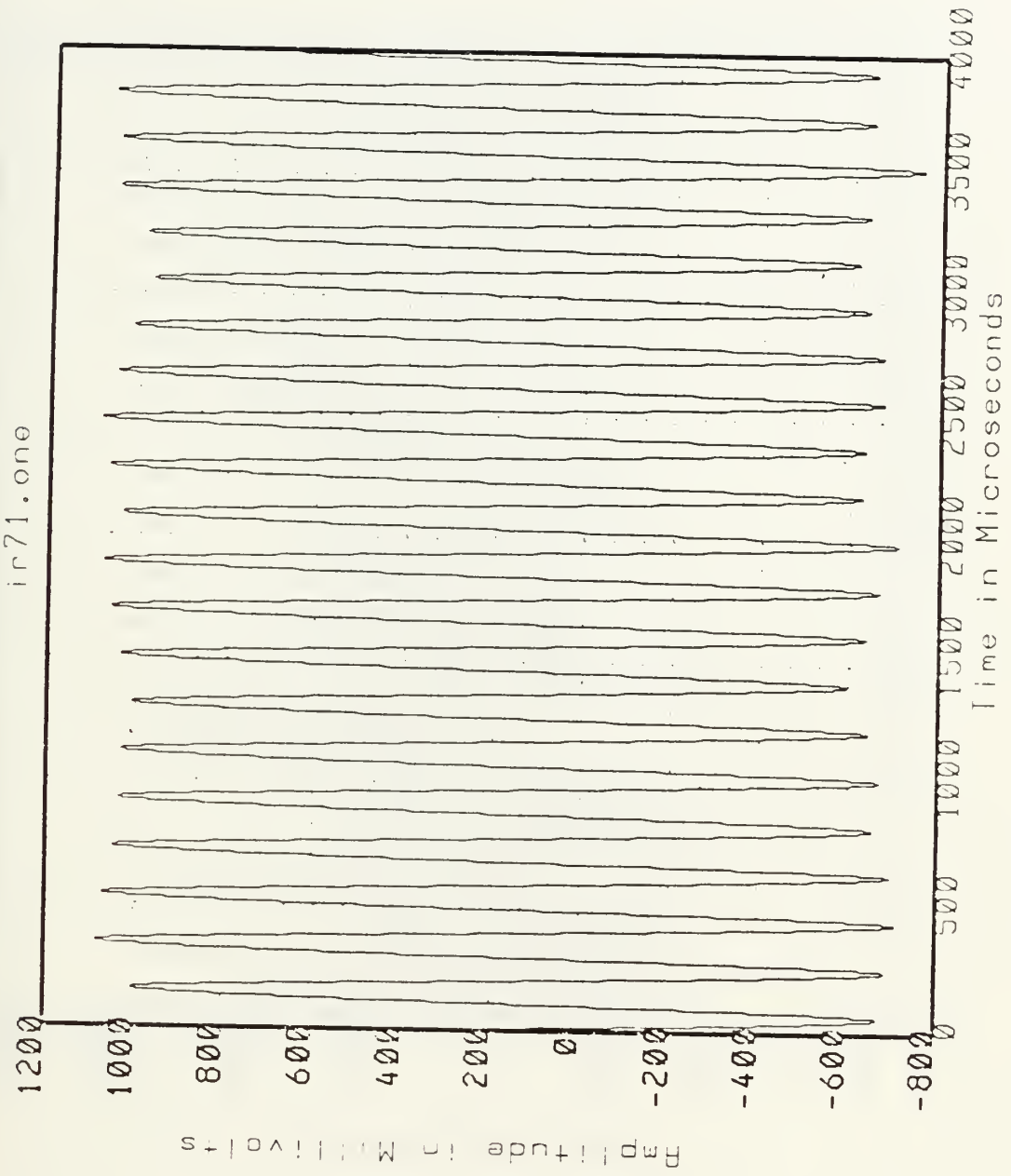

Standard Response of the Lead Array

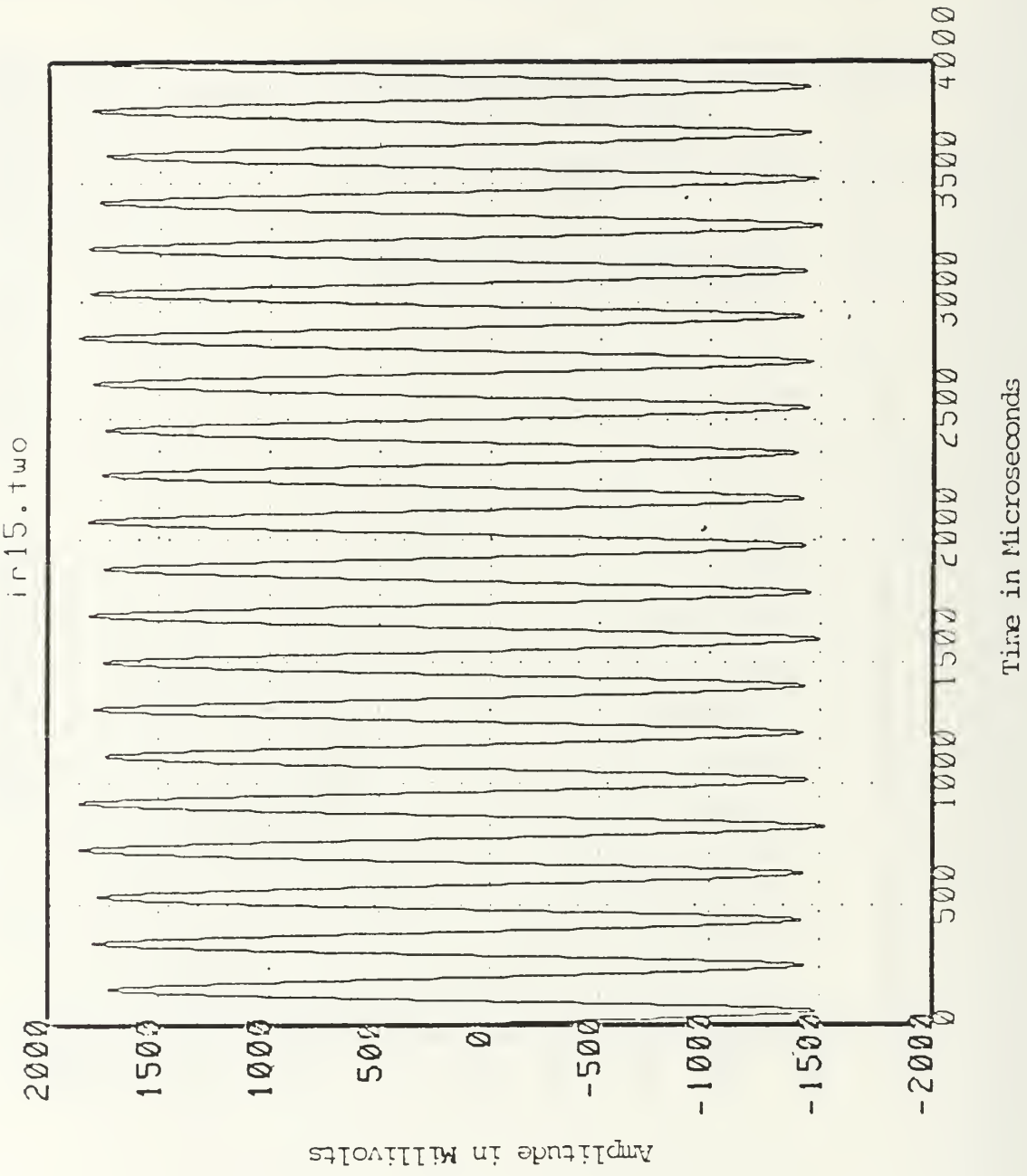

Standard Response of the Lag Array

Impaired Detector on Lead Array

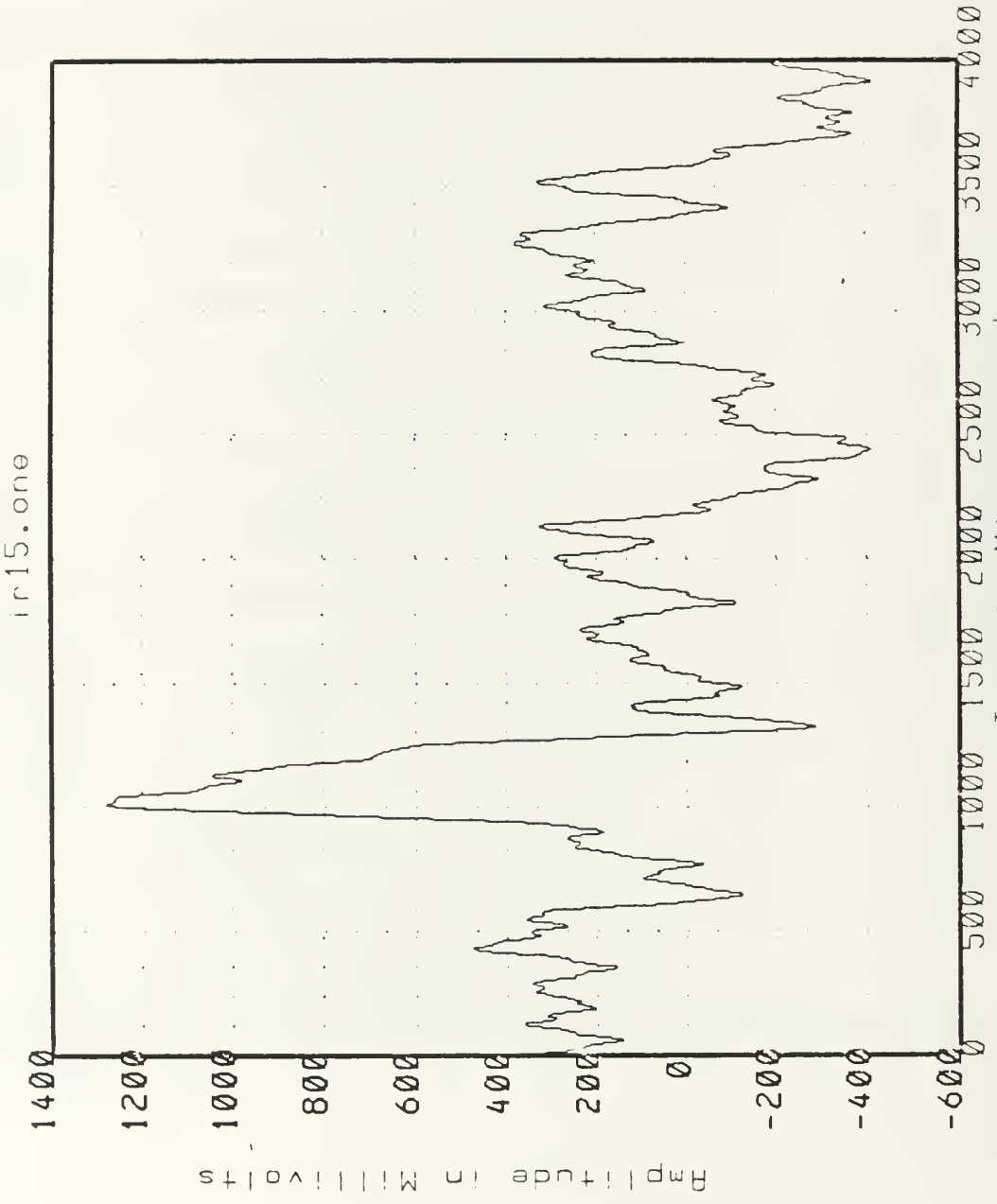

Impaired Detector on the Lead Array

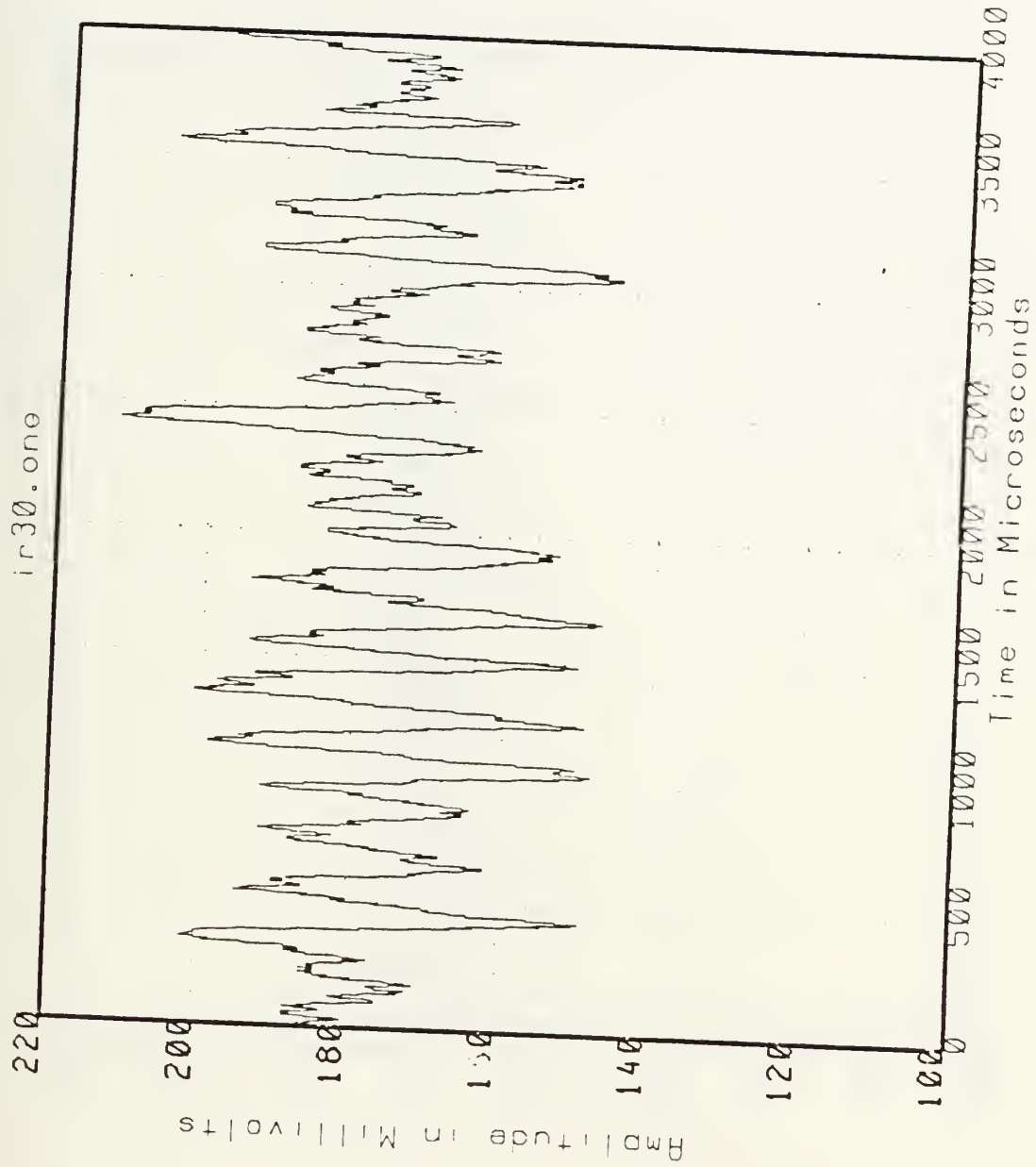

Impaired Detector on the Lead Array

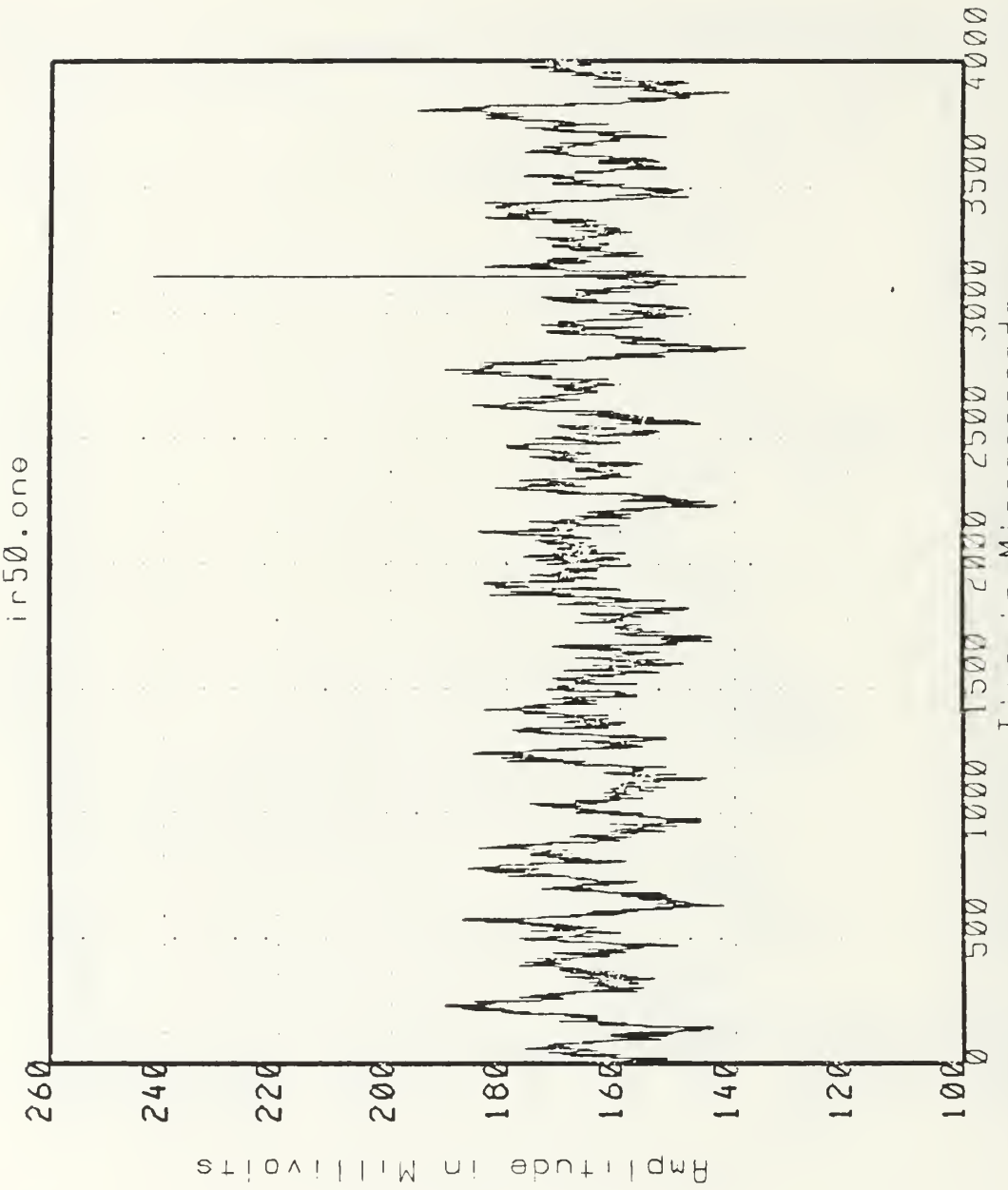

Impaired Detector on the Lead Array

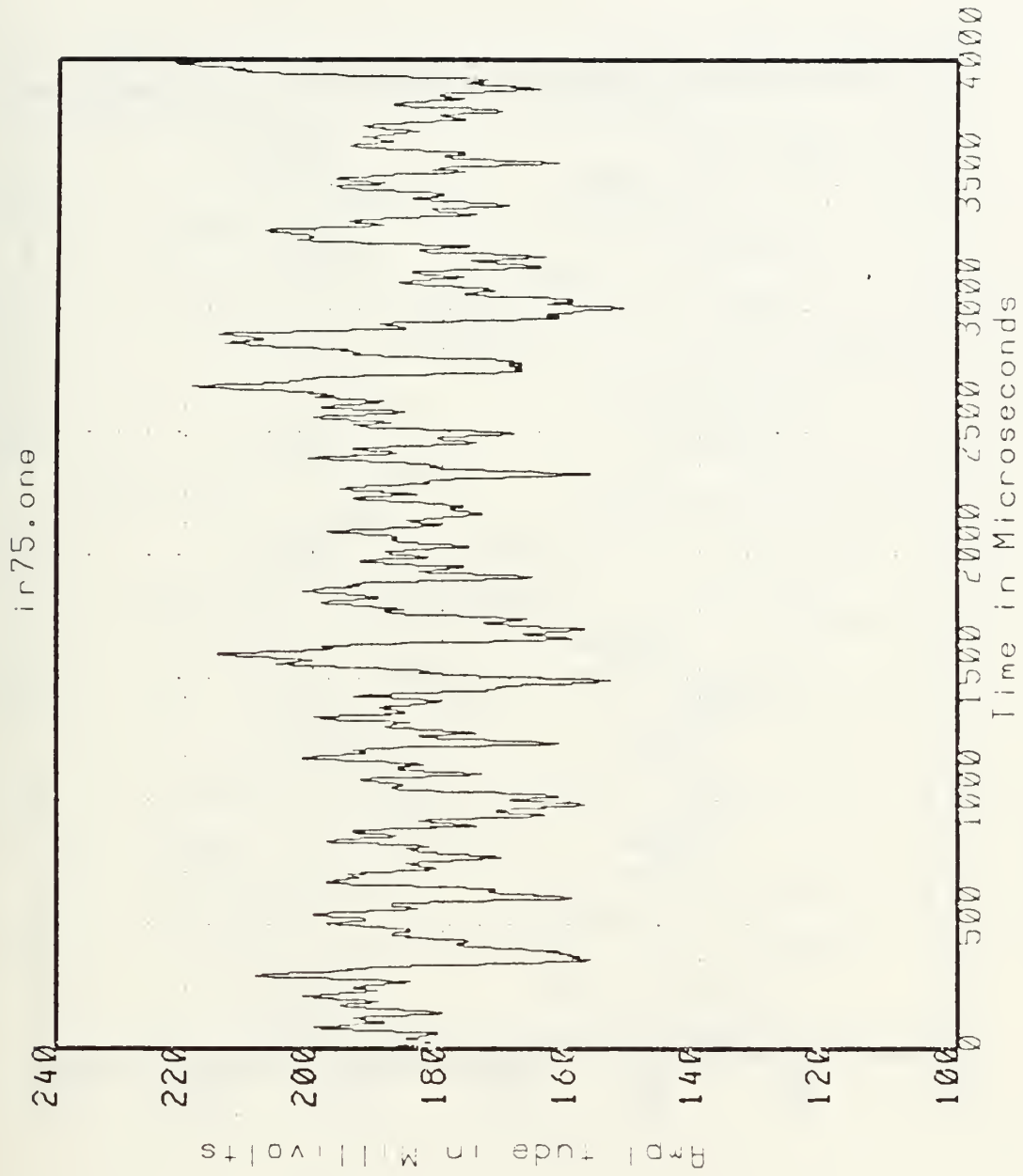

Impaired Detector on the Lead Array

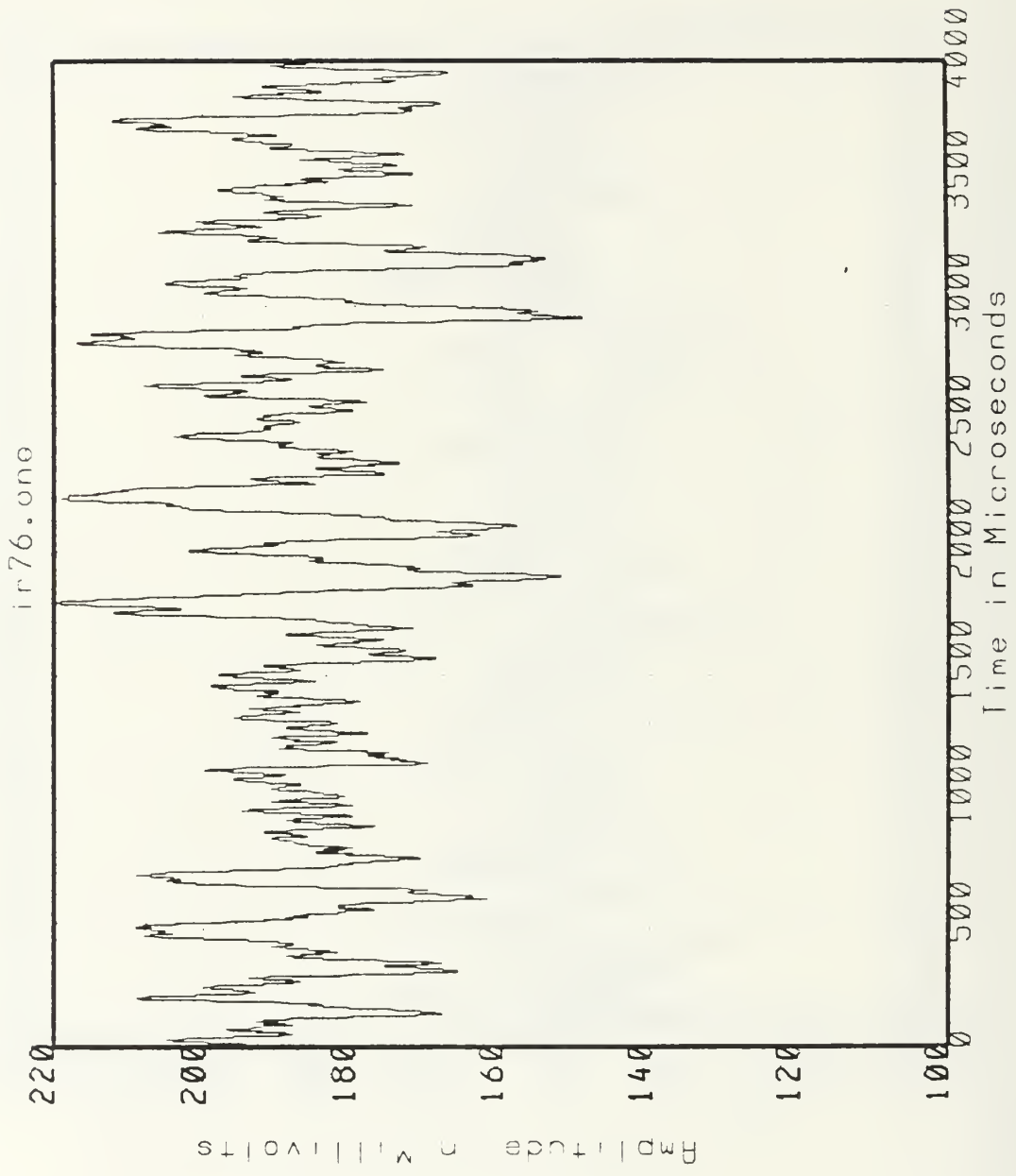

Impaired Detector on the Lead Array

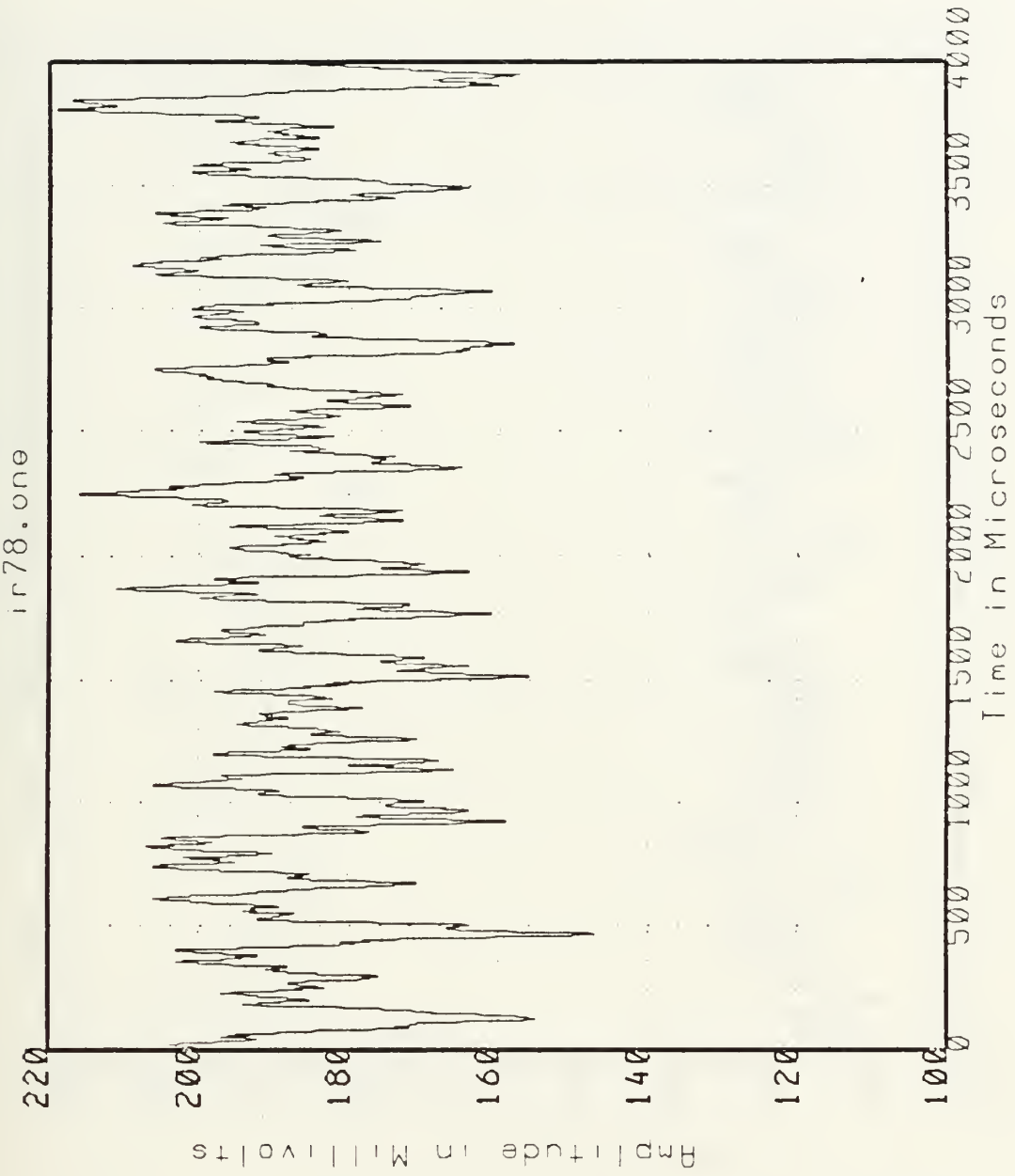

Impaired Detector on the Lead Array

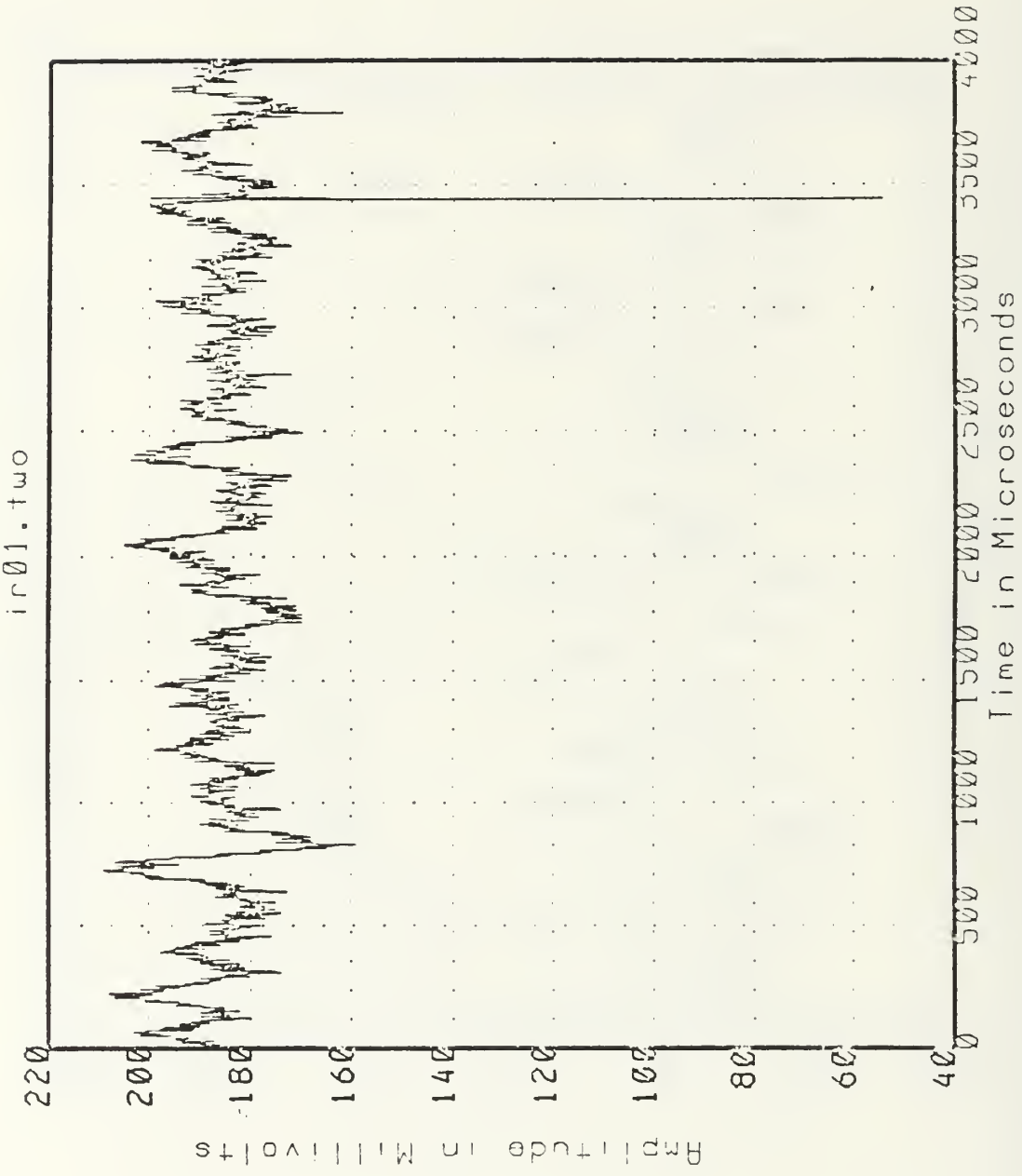

Impaired Detector on the Lag Array

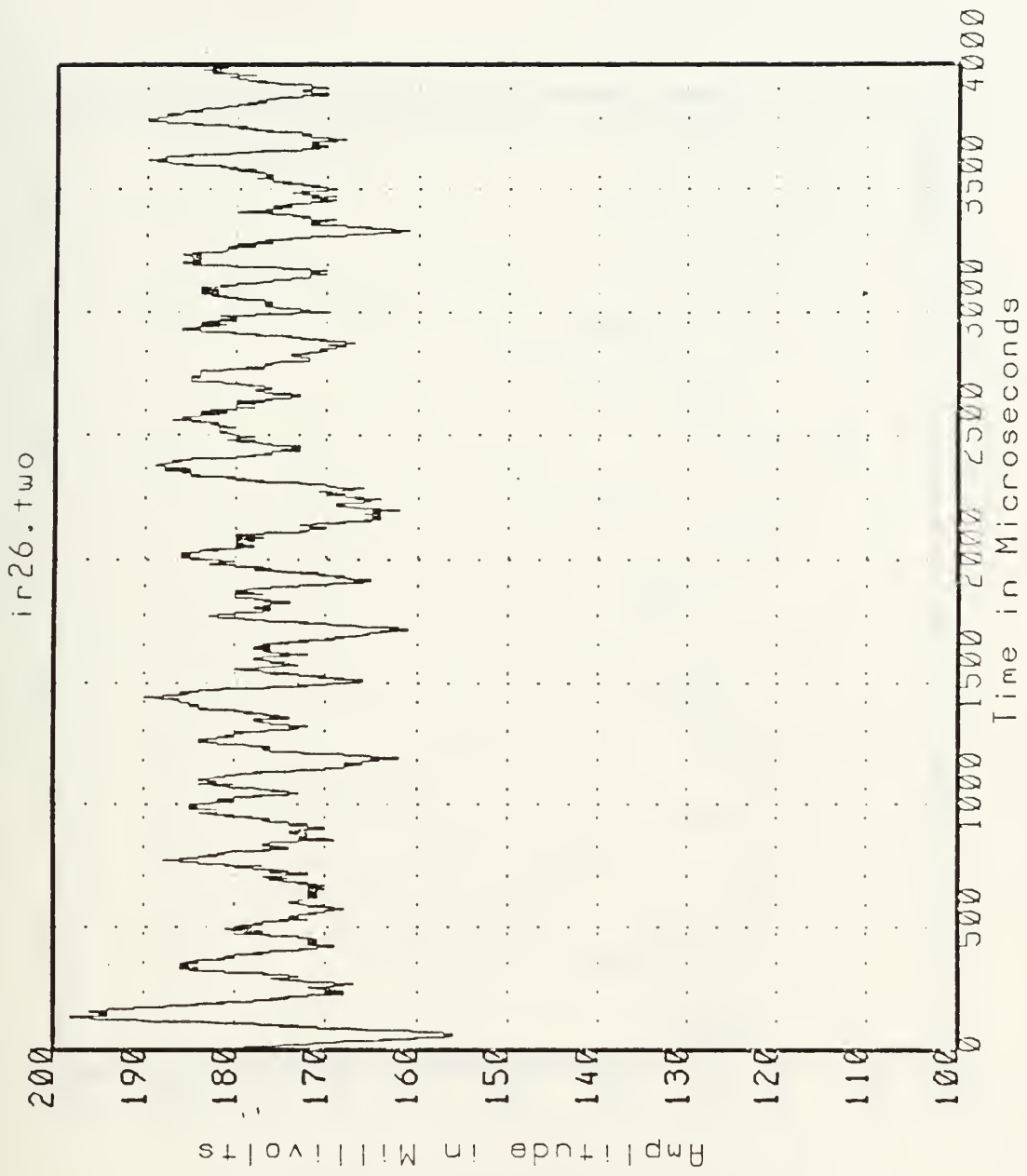

Impaired Detector on the Lag Array

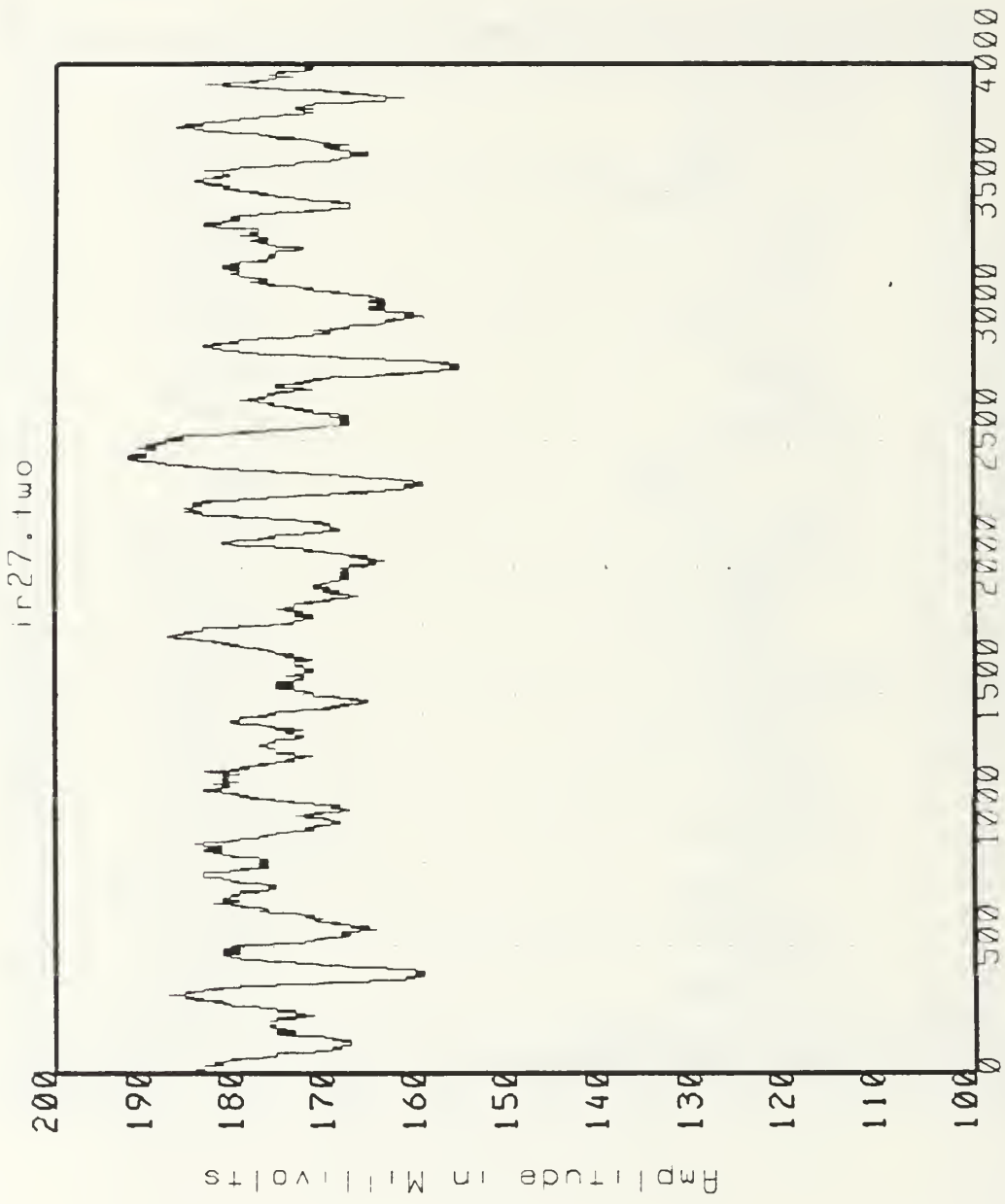

Impaired Detector on the Lag Array

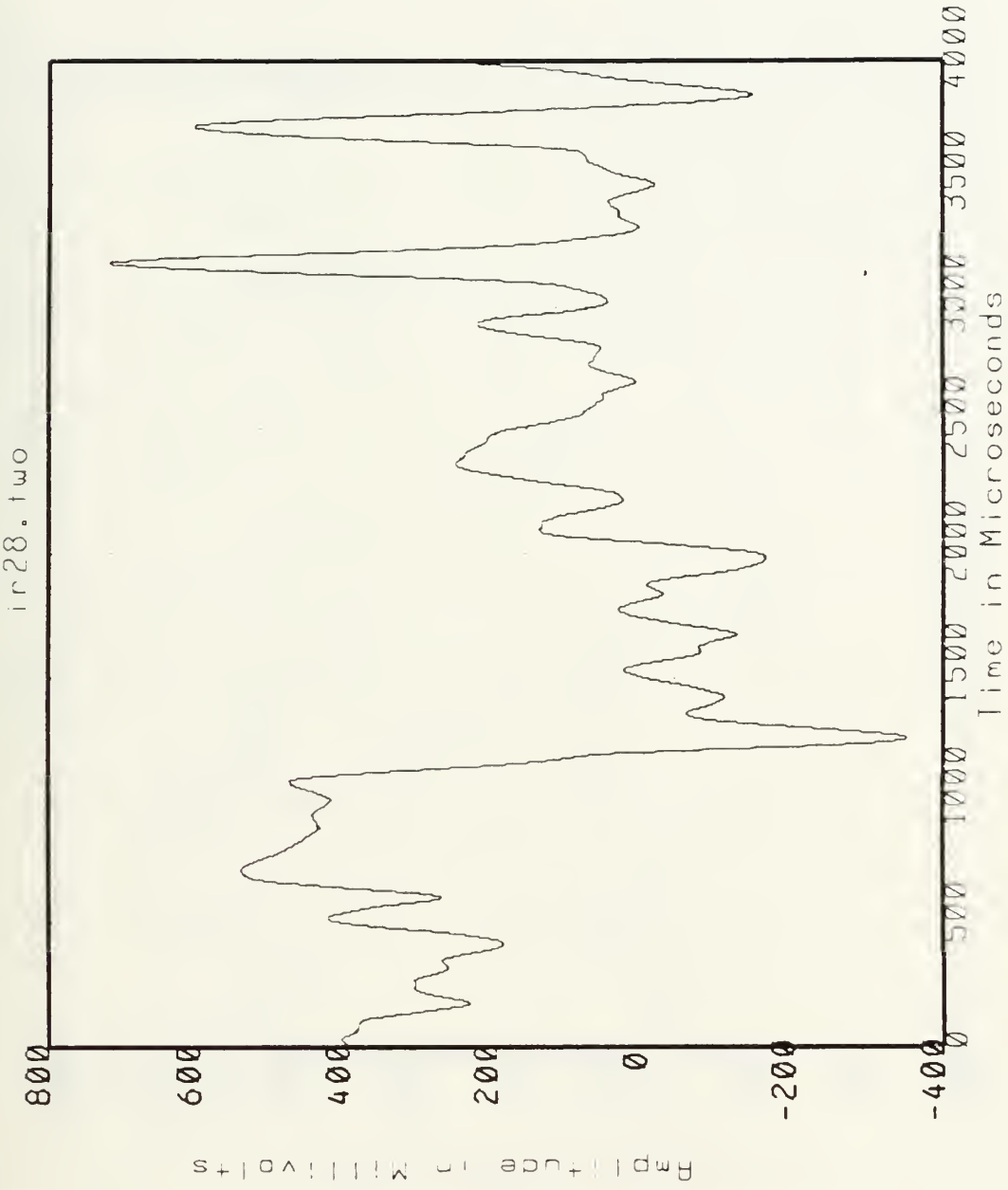

Impaired Detector on the Lag Array

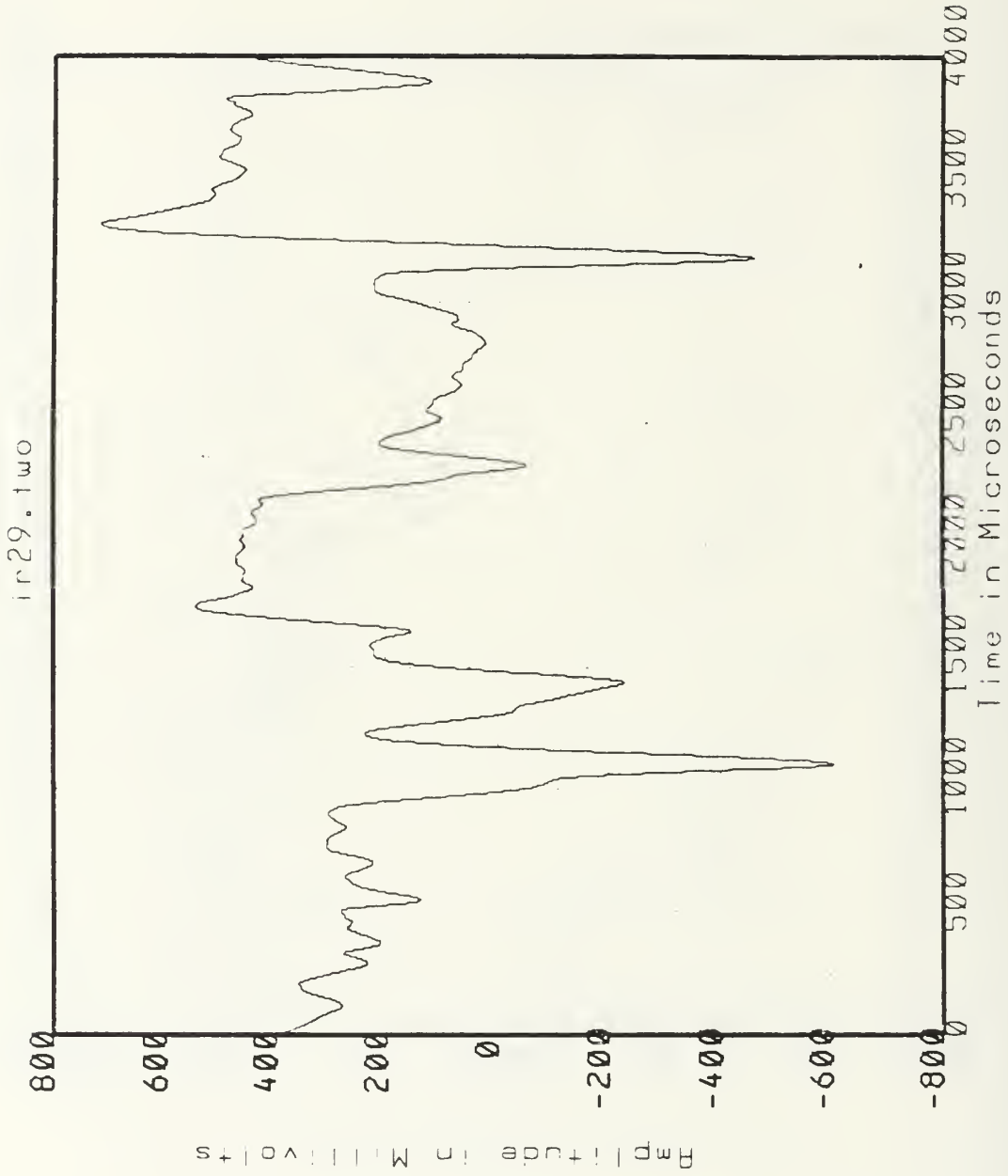

Impaired Detector on the Lag Array

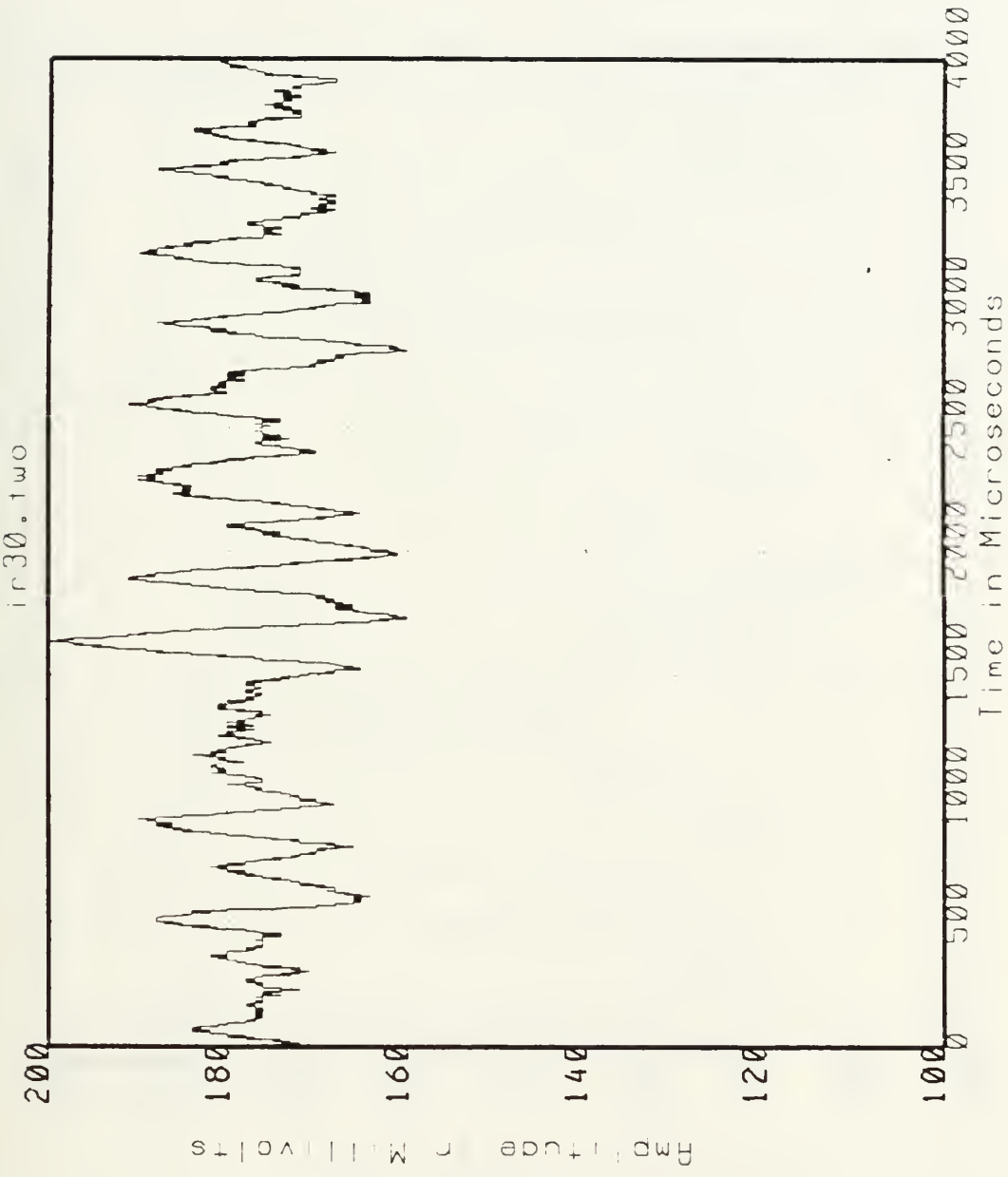

Impaired Detector on the Lag Array

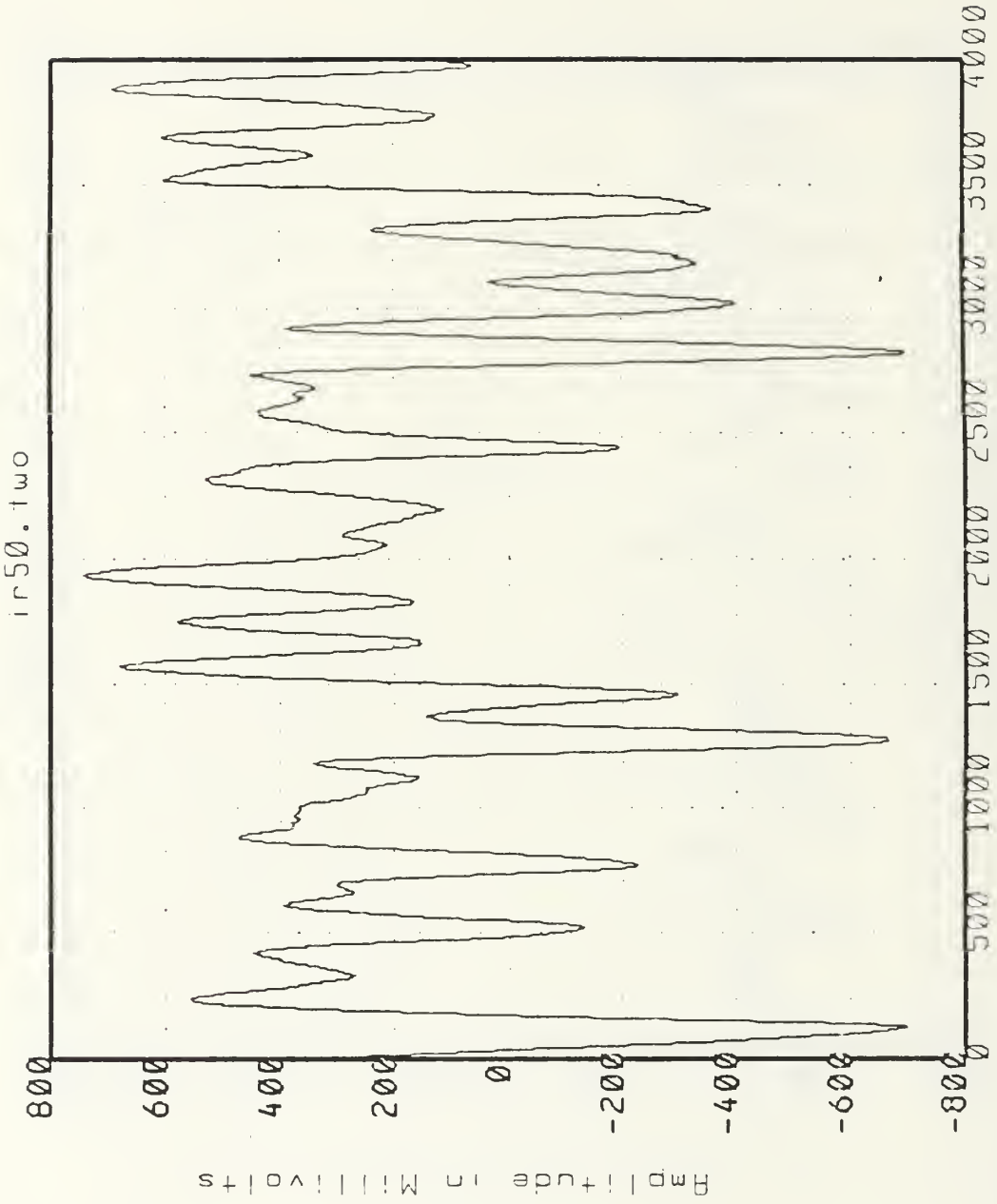

Impaired Detector on the Lag Array

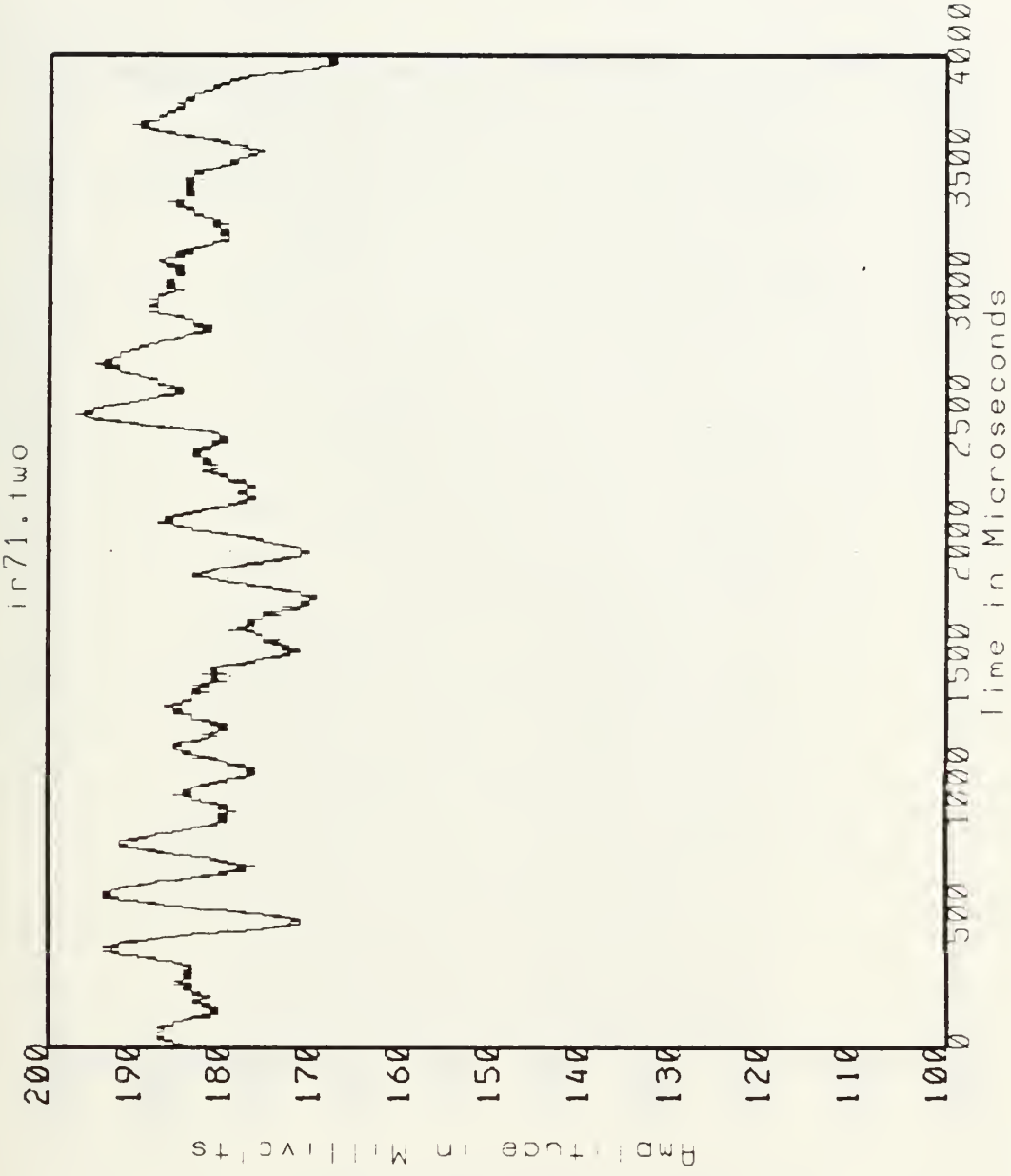

Impaired Detector on the Lag Array

Impaired Detector on the Lag Array

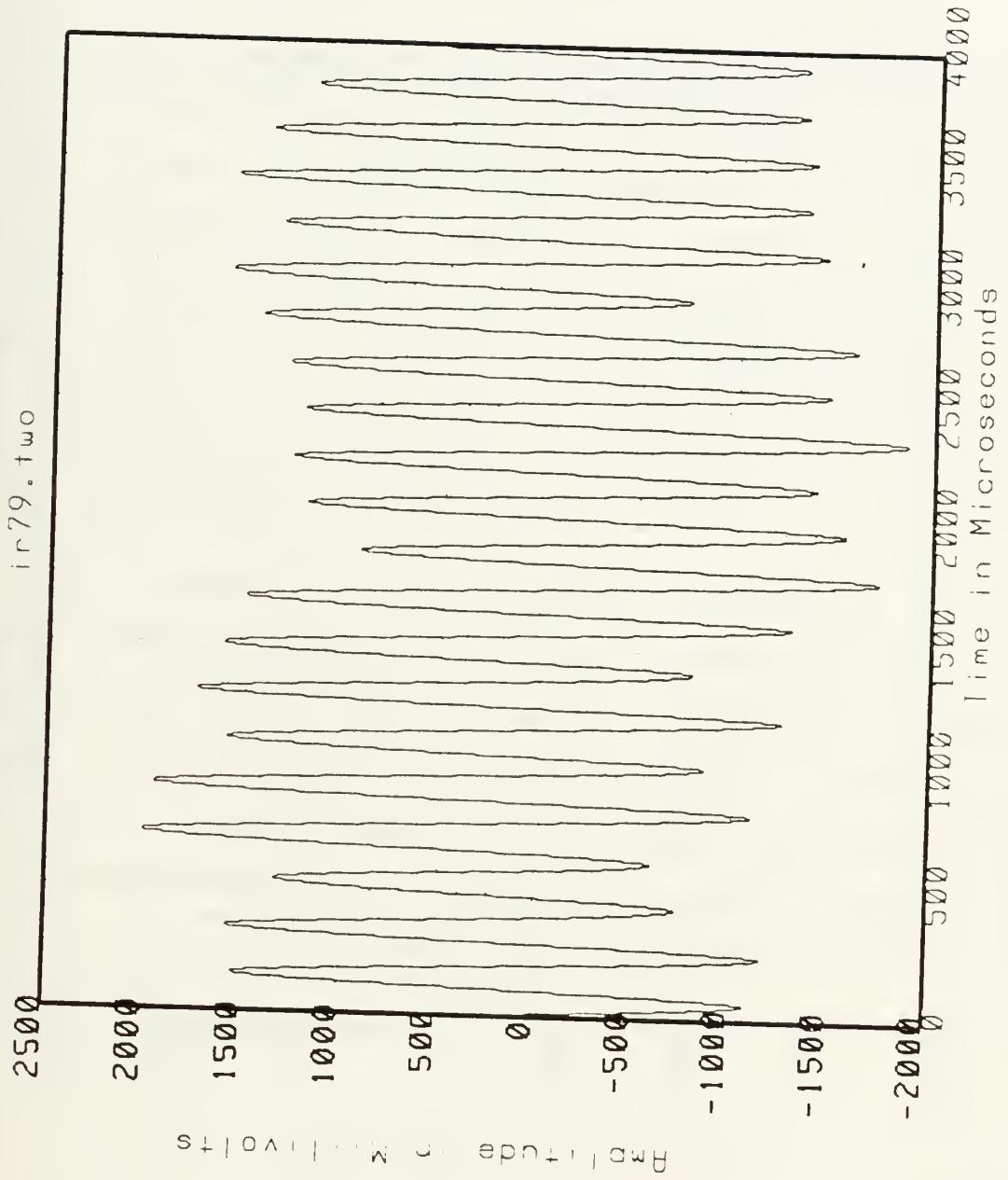

Impaired Detector on the Lag Array

Impaired Detector on the Lag Array

APPENDIX C

COOLDOWN CURVES FOR THE IRSTD

This is a comparison of the cooldown curves between the original ADM and the NPS modified version. The original ADM used a double walled Dewar vacuum flask for thermal insulation with the cooling done by means of a mechanical refrigerator system. This system was defective upon arrival at NPS and it was decided to replace it with a modified one. The new modification made use of a cylindrical chamber filled with liquid nitrogen which flows down into the detector stalk well.

This modification has several advantages over the old system. It eliminated a source of microphonic noise that had been picked up by the detectors, caused by the cryogenic engine. The total time required to reach an operational temperature of 90 K has been reduced from approximately 45 to 10 minutes. Against this advantage must be weighed the necessity to stop and refill with LN after 50 minutes of operation.

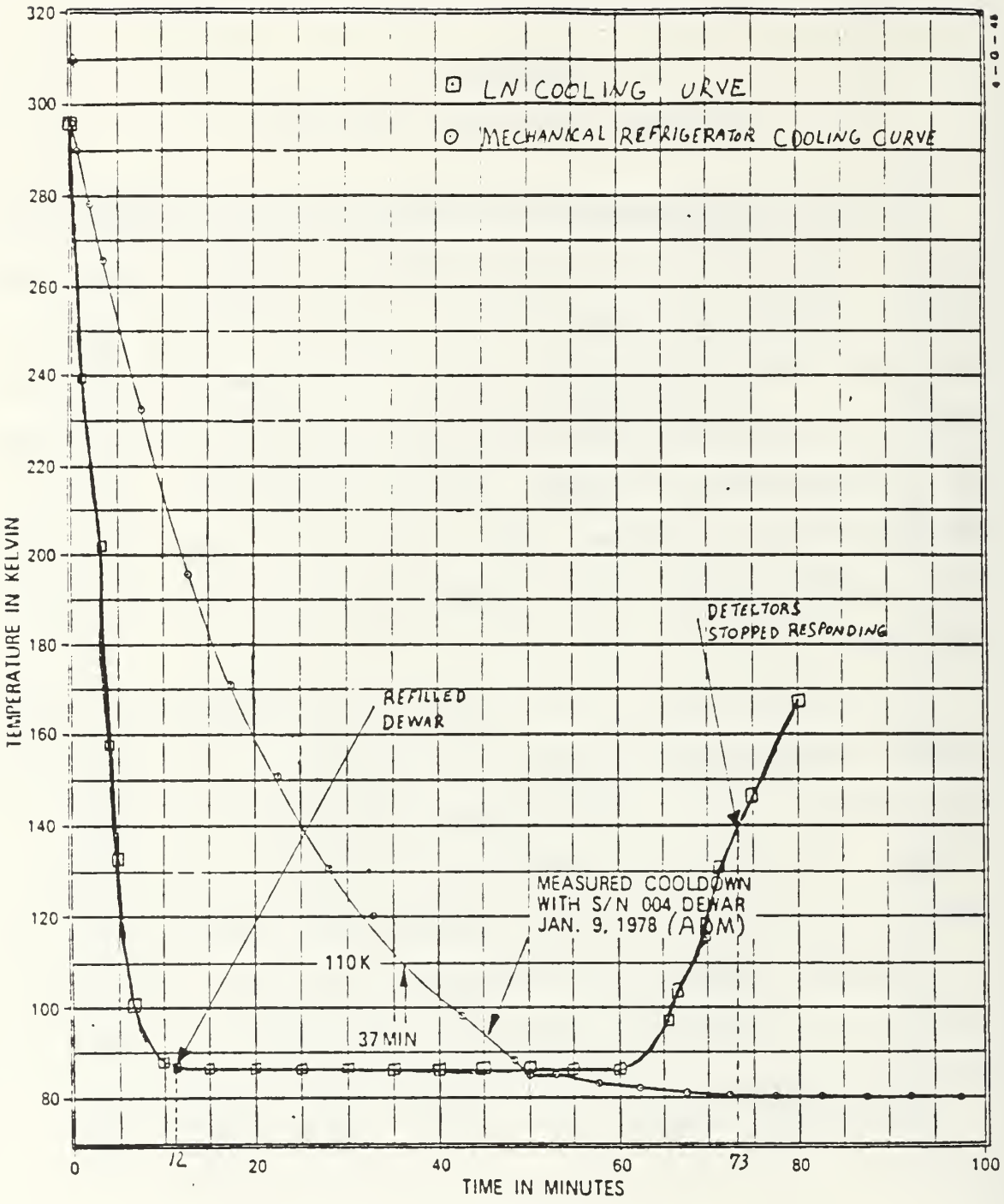

Temperature-Versus-Time Cooldown Curves

APPENDIX D

COMPARISON OF INFRARED TO VISUAL VIEW

This is the comparison of a photograph of the view seen from the door of room Sp-703 on the roof of Spanagel Hall with an detector scan of the same view made by the AN/SAR-8 ADM. The IR shot was made with a lead array detector at 0° elevation angle with a medium sky background. The detector head was focused for the glowbar at a distance of about 15 meters. The sources are labeled on both the photograph and the IR scan as follows:

A . . . . Airvent Pipe

B . . . . Glowbar

C . . . . Clamp Holder

D . . . . Storage Building

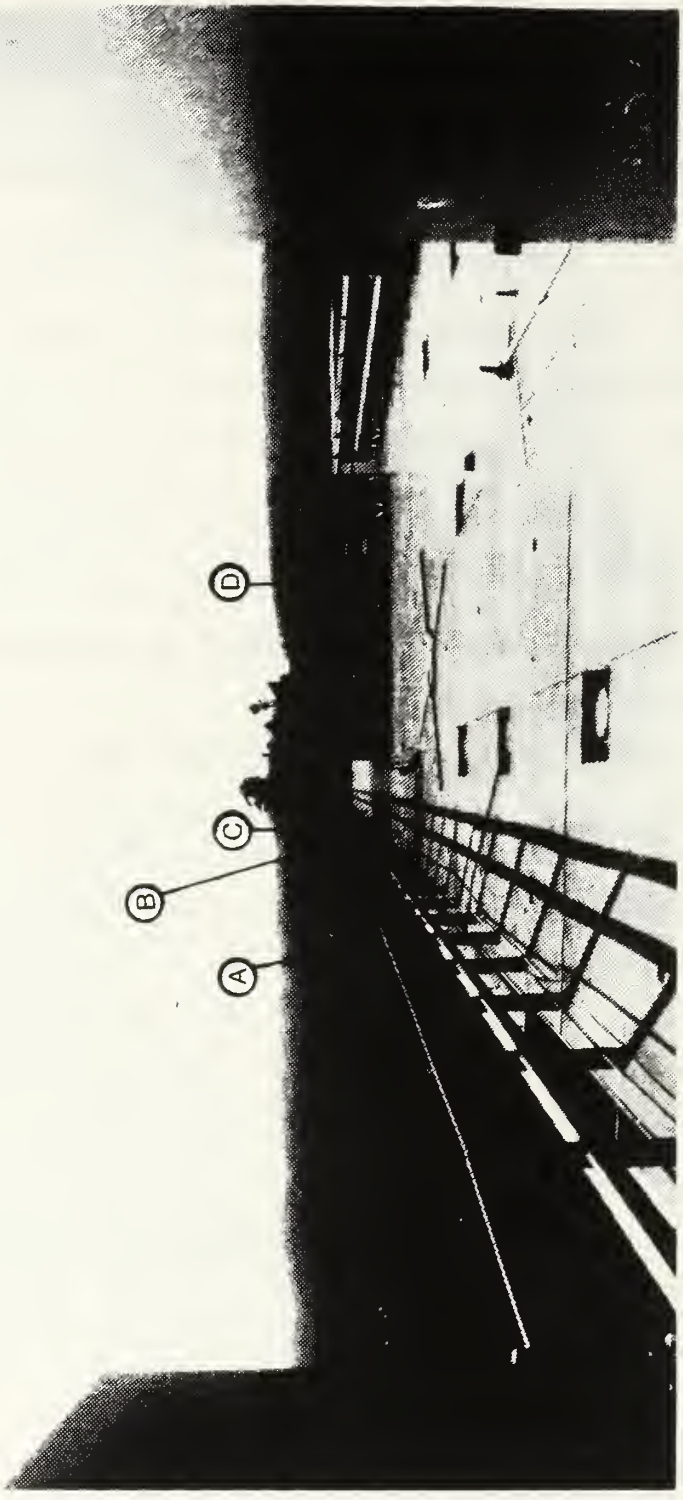

Photograph of View Out Door

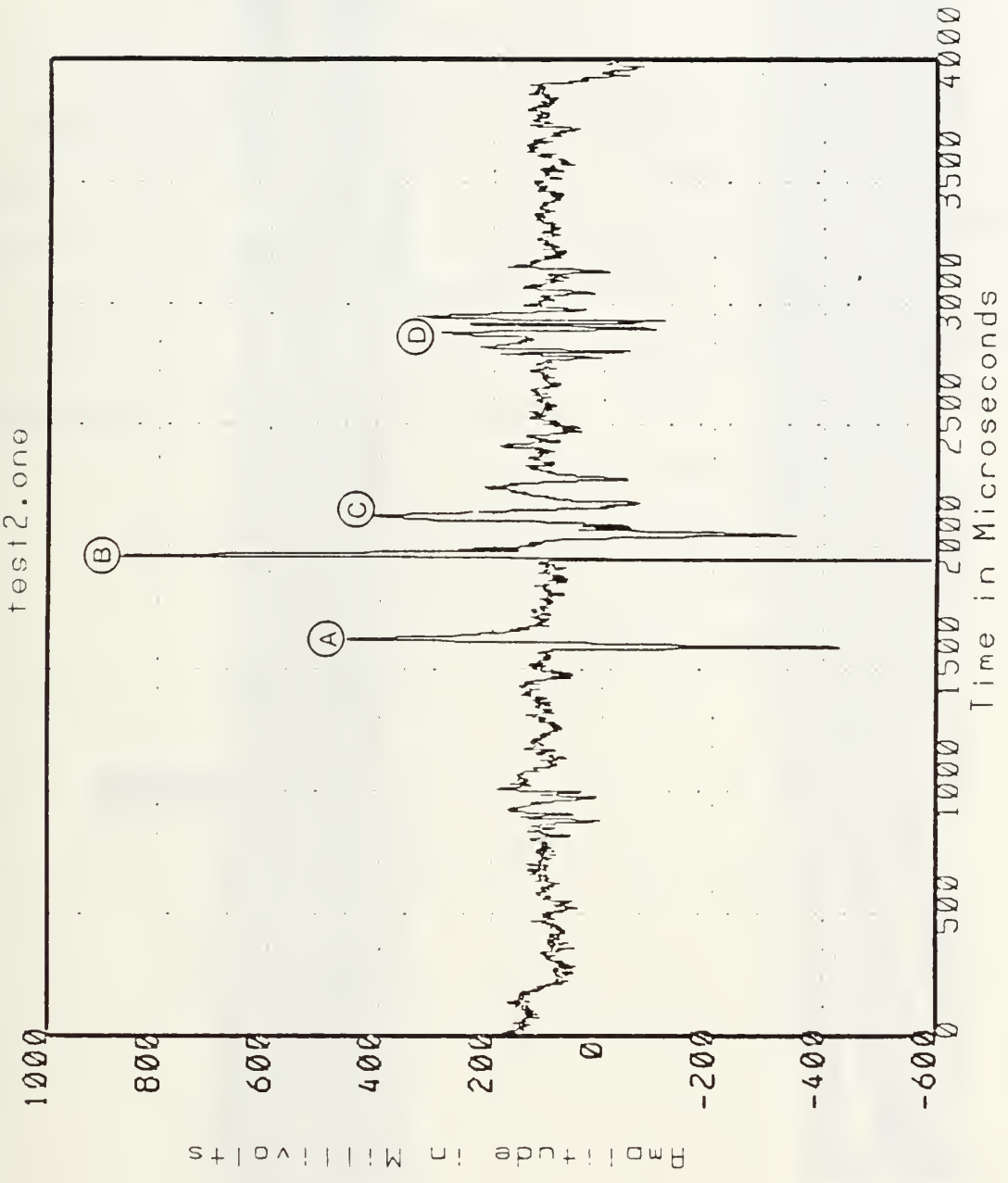

IR Scan Out Door

APPENDIX E

PHOTOGRAPH

This is a photograph of the panoramic view as seen from the designated installation position for the IRSTD on top of the north end of Spanagel Hall. This position will provide all types of IR targets, surface and air. It will also enable background data to be collected on clouds and differing types of fog. Certain aspects of the photograph are labled as follows:

A . . . . Hillside where fog rolls over frequently

B . . . . Monterey Bay

C . . . . Monterey Airport

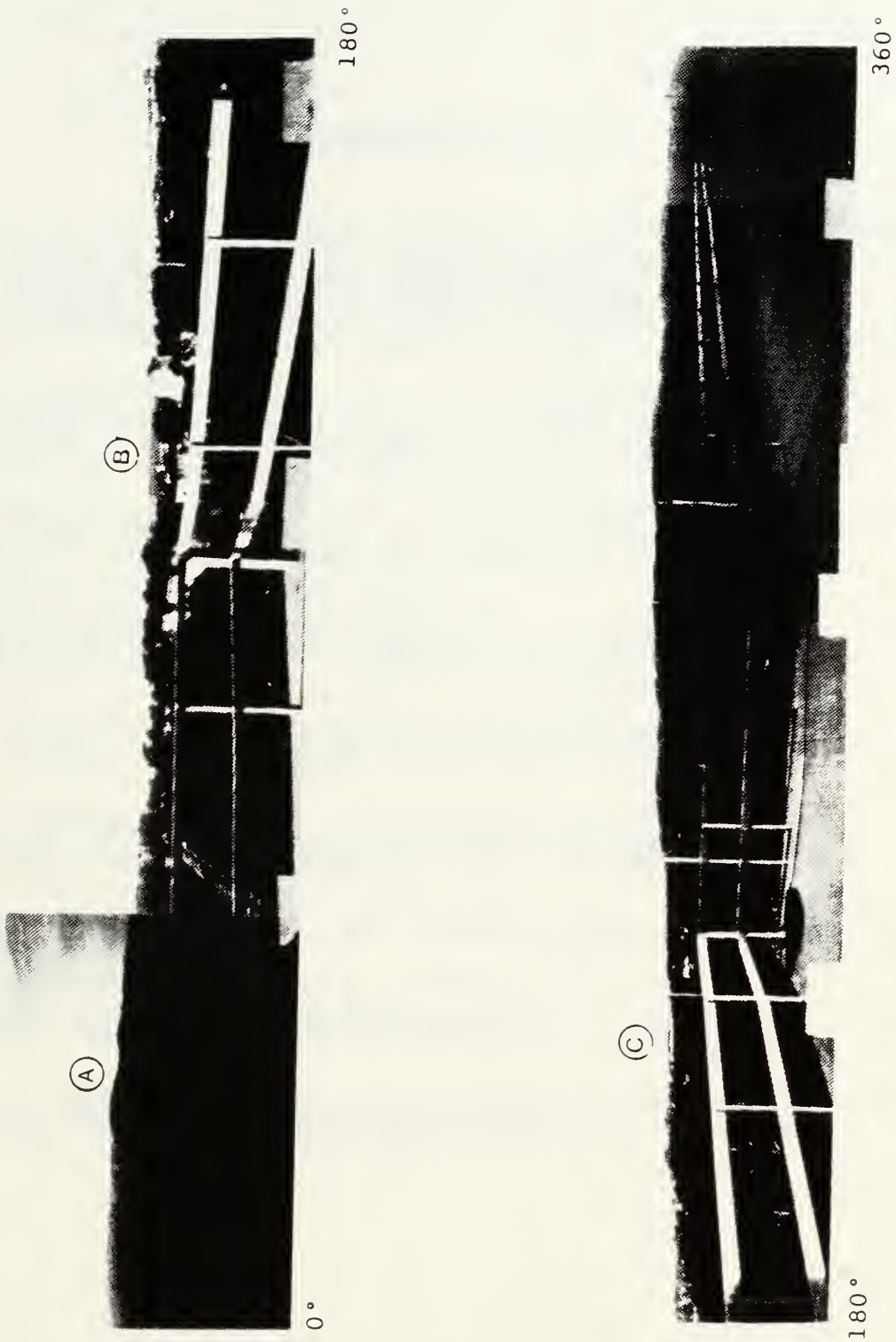

Photograph of Panoramic View

LIST OF REFERENCES

1. Parker, Gary W., Optical Performance Implications of Naval Postgraduate School Modifications to the AN/SAR-8 Infrared Search And Target Designation System, Master's Thesis, Naval Postgraduate School, Monterey, California, September 1986.

2. Naval Electronics Systems Command, The Infrared Search and Target Designation System (IRSTD), p. 10, Government Printing Office, Washington, DC, 1984.

3. SPAR Aerospace Products LTD., In Process Review (IPR) Meeting Data Package, 20 January, 1977, SPAR-R.863, 1977.

4. Devore, Jay L., Probability and Statistics for Engineers and the Sciences, Brooks/Cole Publishing Co., Wadsworth Inc., 1982.

5. The Infrared Handbook, Office of Naval Research, Department of the Navy, Washington, DC, 1978.

6. SPAR Aerospace Products LTD., Minutes of IRST In Process Review (IPR) Meeting, June 21-22, 1977, SPAR-R.863, 1977.

7. SPAR Aerospace Products LTD., Equipment Log, February 19-June 5, 1979.

8. Hudson, R. D., Infrared System Engineering, John Wiley & Sons, Inc., 1969.

9. Truitt, R. W., Fundamentals of Aerodynamic Heating, pp. 4-8, The Ronald Press Company, 1960.

INITIAL DISTRIBUTION LIST

		No. Copies
1.	Defense Technical Information Center Cameron Station Alexandra, Virginia 22304-6145	2
2.	Superintendent Attn: Library, Code 1424 Naval Postgraduate School Monterey, California 93943-5002	2
3.	Superintendent Attn: Department Chairman, Code 61 Naval Postgraduate School Monterey, California 93943-5000	2
4.	Superintendent Attn: Professor A. W. M. Cooper, Code 61Cr Naval Postgraduate School Monterey, California 93943-5000	3
5.	Superintendent Attn: Professor E. C. Crittenden, Code 61Ct Naval Postgraduate School Monterey, California 93943-5000	1
6.	Commander Attn: CDR B. W. Carver, SEA06W1-4 Naval Sea Systems Command Washington, DC 20362-5101	2
7.	LT. Gary R. Ayers 276 Eastern Shores Drive Lexington, Tennessee 38351	3

Thesis
A9953
c.1 Ayers
Calibration and initialization of the NPS modified infrared search and target designation (IRSTD) system.